Green Synthesis, Characterization, and Evaluation of Antimicrobial and Antioxidant Activities of CuO, Co_3O_4, and CuO-Co_3O_4 Composite Nanoparticles using leaf Extracts of *Moringa stenopetala*

Desalegn Tesfa Tefera

A Thesis Submitted to the Department of Applied Chemistry in Partial Requirement for Fulfillment of a Master of Science Degree in Applied Chemistry (Inorganic Chemistry)

Office of the Postgraduate Studies

Adama Science and Technology University

July 2023

Adama, Ethiopia

Green Synthesis, Characterization, and Evaluation of Antimicrobial and Antioxidant Activities of CuO, Co_3O_4, and CuO-Co_3O_4 Composite Nanoparticles using leaf Extracts of *Moringa stenopetala*

Desalegn Tesfa Tefera

Main Advisor: Prof. Tegene Desalegn

Co-Advisor: Akalu Terfa, PhD

A Thesis Submitted to the Department of Applied Chemistry in partial requirement for fulfillment of a master of science degree in Applied Chemistry (Inorganic chemistry)

Office of the Postgraduate Studies

Adama Science and Technology University

July 2023

Adama, Ethiopia

Declaration

I declare that this Master thesis entitled **"Green Synthesis, Characterization and Evaluation of Antimicrobial and Antioxidant Activities of CuO, Co_3O_4, and CuO-Co_3O_4 Composite Nanoparticles using leaf Extracts of *Moringa Stenopetala*"** is my work and has not been submitted to any university for a similar purpose. The references used in this proposal are duly recognized by proper citations.

_____	_____	_____
Name of student	Signature	Date

Recommendation

We, the advisors of this thesis, hereby certify that we have read the revised version of the thesis entitled **"Green Synthesis, Characterization and Evaluation of Antimicrobial and Antioxidant Activities of CuO, Co_3O_4, and CuO-Co_3O_4 Composite Nanoparticles using Leaf Extracts of *Moringa Stenopetala*"** prepared under my guidance by **Desalegn Tesfa Tefera**. Therefore, we recommend the submission of the revised version of the thesis to the department following the applicable procedures.

Main Advisor	Signature	Date
Co-advisor	Signature	Date

Approval Page of M.Sc. Thesis

We, the advisors of the thesis entitled "**Green Synthesis, and Evaluation Of Antimicrobial and Antioxidant Activities of CuO, Co_3O_4, and CuO-Co_3O_4 Composite Nanoparticles using leaf Extracts of *Moringa Stenopetala*"** developed by **Desalegn Tesfa Tefera,** hereby certify that the recommendation and suggestions made by the board of examiners are appropriately incorporated into the final version of the thesis.

Main Advisor	Signature	Date
Co-advisor	Signature	Date

We, the undersigned, members of the Board of Examiners of the thesis by **Desalegn Tesfa Tefera** have read and evaluated the thesis entitled "**Green Synthesis, and Evaluation Of Antimicrobial and Antioxidant Activities of CuO, Co_3O_4, and CuO-Co_3O_4 Composite Nanoparticles using leaf Extracts of *Moringa Stenopetala*"** and examined the candidate during the open defense. This is, therefore, to certify that the thesis is accepted for partial fulfillment of the requirement of the degree of Master of Science in Applied Chemistry (Inorganic chemistry).

Dr. Endale Mulgeta		
Chairperson	Signature	Date
Dr. Enyew Amare		
Internal Examiner	Signature	Date
Dr. Taju Sani		
External Examiner	Signature	Date

Finally, approval and acceptance of the thesis are contingent upon the submission of its final copy to the Office of Postgraduate Studies (OPGS) through the Department Graduate Council (DGC) and School Graduate Committee (SGC).

Department Head	Signature	Date
School Dean	Signature	Date
Office of Postgraduate Studies,	Signature	Date

Table of contents

LIST OF TABLES

Tables Page

LIST OF FIGURES

Figures Page

LIST OF ABBREVIATIONS/ACRONYMS

Co_3O_4	Cobalt oxide
CuO	Copper oxide
DLS	Dynamic light scattering
DMSO	Dimethyl sulfoxide
DPPH	2, 2-Diphenyl-1-picrylhydrazyl hydrate
eV	ElectronVolt
FTIR	Fourier transforms infrared
HRTEM	High-resolution transmission electron microscopy
MO	Metal oxide
NPs	Nanoparticles
NaOH	Sodium Hydroxide
ROS	Reactive oxygen species
SEM	Scanning electron microscopy
TEM	Transmission electron microscopy
TGA	Thermal gravimetric analysis
UV-VIS	Ultraviolet-visible spectroscopy
WHO	World health organization
XRD	X-ray diffractions

ACKNOWLEDGMENT

To begin, I would like to express my gratitude to the divine Creator for providing me with everything I prayed for. I could not have completed this work without the assistance of my mentor, Prof. Tegene Desalegn, for all of his passion, expertise, and scrupulous focus on particulars served as a motivation and guided me through every step of this project, starting from the proposal's inception to the final draft of this work I have a deep love and much appreciation. I would also like to thank my co-adviser, Dr. Akalu Terfa, for his advice and support in keeping my progress on track. Next, I would to thank Mizan Tepi University, Colleague of Natural and Computational Science, Department of Chemistry for giving me a Scholarship opportunity.

I would also like to thank the Department of Applied Biology for allowing me to use (SEM) scanning electron microscopy, the Department of Materials Science for allowing me to use XRD instruments, and Addis Ababa Science and Technology University, College of Natural Science for the dedication of UV-Vis Spectroscopy, Bahir Dar University for their support in FTIR Analysis, Adama Public Health Referral and Research Laboratory Center for antibacterial activity analysis experiment.

Also, I would like to thank Adama Science and Technology University, the School of Applied Natural Science, Department of Applied Chemistry for facilitating facilities and providing financial support for all laboratory works. My thanks also go to the research and technical assistants at the Applied Chemistry Department laboratory for providing me with the necessary support to complete the program. Finally, Let My thanks also go to my parents and friends for their love, assistance, and guidance throughout my study and research work.

.

ABSTRACT

The present work reports the green synthesized CuO NPs, Co_3O_4 NPs, and CuO-Co_3O_4 composite nanoparticles using an extract from Moringa stenopetala leaves, which were designed as agents for antioxidant and antimicrobial purposes. The nanoparticles were thoroughly analyzed using various spectroscopic methods such as XRD, UV-Vis, SEM, FT-IR, and TGA. Based on the UV-Vis data, the energy band gaps of the CuO NPs, Co_3O_4 NPs, and CuO-Co_3O_4 composite NPs were determined to be 3.32eV, 3.36 eV, and 3.66 eV, respectively. The XRD analysis revealed that the CuO NPs had a monoclinic crystal structure with a spherical shape and an average crystallite size of 11.59 nm. Additionally, the Co_3O_4 NPs exhibited a cubic crystal structure with a spinel structure and an average crystallite size of 12.25 nm. Meanwhile, the CuO-Co_3O_4 nanocomposites had an average crystal size of 9.53 nm. The SEM images revealed CuO NPs has heterogeneous composition with large granular particles due to aggregation or overlapping, while Co_3O_4 NPs is non-uniform cubic shape and size, with agglomeration due to encapsulation and hydrogen bonding, and for CuO-Co_3O_4 composite NPs, inhomogeneity of particles, with both spherical and irregular geometries and different sizes. The FT-IR confirms the bioactive molecules such as flavonoids, tannins, terpenoids, steroids, glycosides, saponins, and phenols, *that were actively involved during the synthesis process. The antibacterial effects of the produced nanoparticles were tested against Gram-negative (Escherichia coli and Pseudomonas aeruginosa) and Gram-positive (Staphylococcus aureus and Streptococcus pyogenes) bacterial strains using the agar-well diffusion method. CuO-Co_3O_4 composite NPs showed better inhibitory activity than CuO NPs and Co_3O_4 NPs against the selected bacterial species (Escherichia coli, Pseudomonas aeruginosa, and Streptococcus pyogenes). Similarly, the antioxidant activities of the synthesized NPs were evaluated using DPPH assays. The results confirmed that the CuO-Co_3O_4 composite NPs have excellent inhibitory activity compared to CuO NPs and Co_3O_4 NPs. The results of this study suggest that the CuO-Co_3O_4 composite NPs hold great potential for various applications, given their superior inhibitory and radical inhibitory activity.*

***Keywords**: Antimicrobial activity; Antioxidant activity; CuO-Co_3O_4 composite NPs; Moringa stenopetala*

CHAPTER ONE

INTRODUCTION

1.1 Background of the study

"Nanotechnology" is an emerging technology of objects, that is, the technological expertise of objects with the smallest dimensions starting from some nanometres to much less than one hundred nanometres. This size range is typically connected to colloids, micelles, polymer molecules, phase-separated domains in block copolymers, and other structures in chemistry. Commonly, very large molecules, or aggregates of many molecule structures including buck tubes, silicon nanorods, and compound semiconductor quantum dots have emerged as mainly exciting training of nanostructures Whitesides, 2005). Nanotechnology is the creation, manufacturing, and use of structures, devices, and systems through control of size and shape at the nanoscale scale (Engineering & Kamal, 2017).

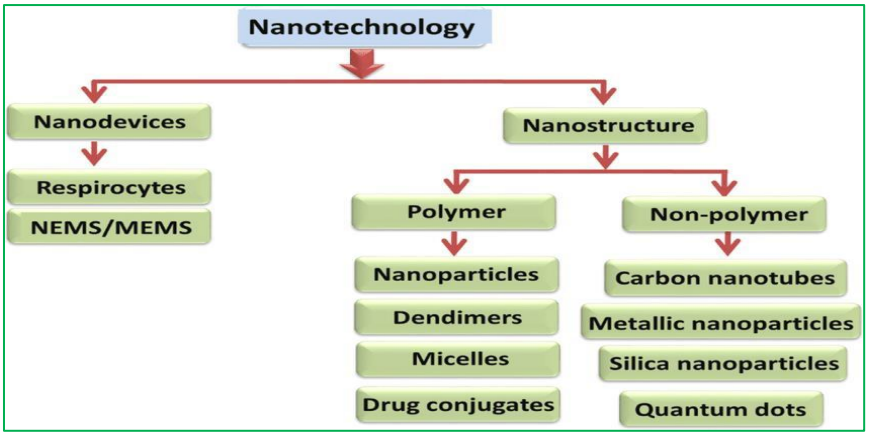

Figure 1: Classification of nanotechnology

Nanomaterials (NMs) have become more popular in the 21st century because of their versatility and ablity to be treated as major research focus areas in the sectors of energy, water, and water sanitation(Mungondori et al., 2018), medical(Mauricio et al., 2018), agriculture(Rastogi et al., 2019), material science, and cosmetics. The most basic definition of nanotechnology is the creation of materials at the atomic, molecular, and supermolecular levels, or more precisely, the use of nanomaterials (NMs) with dimensions of 1-100 nm in a variety of basic and applied

disciplines. The word "nano" is a diminutive form of the Greek word "Nanos," which also means dwarf, and it refers to an estimated one billionth of a. (10^9) meters in diameter. It encompasses frameworks with sizes above and below normally apparent measurements (i.e. > 1 nm and ≤100 nm)(Pantidos, 2014).

Due to their distinct, flexible, and adaptive optical, mechanical, electrical, biocatalytic, and magnetic properties superior to those of their bulk form, NMs have gained importance in technological advances. The unique properties of NMs, which can be tailored to their application, are due to their large surface area and large size. Furthermore, the physical attributes of nanoparticles such as their dimensions, configuration, and makeup have a significant impact on their reactivity, durability, and other characteristics, making them ideal for a broad range of commercial and residential applications(Mutukwa & Taziwa, 2022).

These purposes include environmental conservation, imaging, medical treatments, energy generation, catalysis, aesthetics, and therapeutic uses. Because of the wide range of unique qualities and uses that metal oxide nanoparticles, such as copper oxide (CuO), zinc oxide (ZnO), and titanium dioxide (TiO_2) are among the most studied NMs(Mutukwa et al., 2022).

Green nanotechnology is the branch of green chemistry based on the twelve principles of green chemistry and is an effective replacement for conventional nanochemistry. There are three different methods to synthesize NPs: chemical, physical, and biological methods. The chemical method requires chemical reagents with special temperature and pressure maintenance to function properly. This method also produces toxic by-products. Consequently, it is not a sustainable method. The physical approach does not include solvent contamination, but furnace operation and maintenance call for very high temperatures and pressures. As a result, this approach is also bad because it harms the ecosystem. The biological approach is the most effective for creating NPs(Riaz et al., 2022).

By reducing the metal ion with plant extract, metal ions are transformed into metal atoms in this process. The biomolecules in the plant extract function both as a capping and reducing agent. This procedure is carried out at standard pressure and temperature and is relatively straightforward. Metallic nanoparticles are also made by fungi, and the proteins are responsible for keeping them stable. Additionally, several types of algae are employed to convert metal ions into rod-shaped metal atoms. It is challenging to maintain a culture media for both fungi and

algae. Therefore, using metal ions along with plant extract is the favored way to make metal NPs.(Riaz et al., 2022)

A plant extract is a substance or active ingredient with a desired property obtained from plant tissue by treatment for a specific purpose. Extracts obtained from plants are versatile and can be employed across multiple industries, including health and wellness products, therapeutic medicine, cosmetics, food processing, and as chemical substitutes. These extracts contain an array of bioactive compounds that exhibit antioxidant effects, such as flavonoids, catechins, phenols, quercetin, anthocyanins, tocopherol, rutin, lycopene, chlorogenic acid, caffeic acid, ferulic acid, p-coumaric acid, protocatechuic acid, vitamin C, vitamin E, carotenoids, -carotene, myricetin, kaempferol, zeaxanthin, carnosine, sesamol, rosmarinic acid, carnosic acid, and carnosol(Awad et al., 2021).

Moringa is a tropical plant of the Moringaceae family. Among the different species, *Moringa oleifera* and *Moringa stenopetala* are the best-known and most-used species of Moringa plant. Due to Moringa's versatile behavior, several impressive names have been given such as B. "Tree of Life", "Tree that never dies", "Magic Tree", "Tree of Paradise" and "Mother's Best Friend". Native to southern Ethiopia and northern Kenya, the *Moringa stenopetala* is also known as the East African Moringa tree. Significant nutritional and therapeutic benefits are provided by the tree. Extracts from the *M. stenopetala* plant have recently been used in the manufacture of nanoparticles as capping and reducing agents. The reduction and stability of metal ions to create nanoparticles depend critically on the reduction properties of the plant's components. (Awad et al., 2021).

1.2 Statement of The Problem

Infectious diseases are among the global health problems that cause the highest mortality rate and require intervention. The increasing trend toward microbial resistance to existing antibiotics has compounded the challenge. The ability of pathogenic microbes to adapt to multiple synthesized antimicrobial agents is very rapid and therefore requires a continuous search for new antimicrobial agents. Therefore, it's essential to search for alternative drug candidates to mitigate the growing multidrug-resistant bacterial infections.

Additionally, the development of extremely reactive chemical species, or "free radicals," in the body is thought to be the primary cause of the diseases. Among the free radicals, the most notable are the reactive oxygen species (ROS), as well as the superoxide anion radical (O_2^{-}•), the hydroxyl radical (HO•), and the non-radical molecule hydrogen peroxide (H_2O_2), all of which are generated in the body through metabolic processes or enter the body from external sources.

Antioxidants, a class of useful substances that stabilize or inactivate free radicals to protect cells from oxidative damage, work to combat the buildup of ROS in the body. In this context, the synthesis and application of metal-based nanoparticles have gained interest in the search for alternative drugs to treat bacterial infections and alleviate the observed oxidative stress. In this particular study, we will synthesize CuO, Co_3O_4, and CuO-Co_3O_4 nanocomposite NPs using phytochemicals from the *Moringa stenopatala* plant extract and evaluate the antibacterial and antioxidant activities of the resulting nanoparticles. This study will provide answers to the following research questions.

1) Does *Moringa stenopetala* plant extract have the essential phytochemical composition used for various medicinal applications?
2) Is *Moringa stenopetala* plant extract an efficient method for the biosynthesis of CuO NPs, Co_3O_4 NPs, and CuO-Co_3O_4 nanocomposite?
3) Do the synthesized CuO NPs, Co_3O_4 NPs, and CuO-Co_3O_4 nanocomposite with *Moringa stenopetala* plant extract have enhanced antimicrobial and antioxidant effects?

1.2 Objective of The Study

1.2.1 General Objective of The Study

The primary aim of this research is to synthesis, analyze, and assess the antimicrobial and antioxidant effects of copper oxide, cobalt oxide, and copper oxide-cobalt oxide nanocomposites using *moringa stenopetala* plant leaf extract.

1.2.2 Specific Objectives of The Study

1. To assess the phytochemical composition of the plant extract.

2. To synthesis CuO NPs, Co_3O_4 NPs, and CuO-Co_3O_4 nanocomposite by using *moringa stenopetala* leaf extract.
3. To characterize the synthesized NPs and nanocomposites using XRD, SEM, FTIR, TGA, and UV-Vis spectroscopic techniques.
4. To evaluate the antimicrobial effects of the biosynthesized CuO NPs, Co_3O_4 NPs, and CuO-Co_3O_4 nanocomposites using the disc diffusion method against gram-positive and gram-negative bacterial strains.
5. To evaluate the antioxidant properties of CuO NPs, Co_3O_4 NPs, and CuO-Co_3O_4 nanocomposite using the DPPH assay method.

1.3 Significance of The Study

Firstly, The research focuses on the synthesis of CuO NPs, Co_3O_4 NPs, and CuO-Co_3O_4 nanocomposite using *Moringa stenopetala* leaf extract as a reducing agent. This novel approach provides a more eco-friendly and cost-effective method of synthesizing nanoparticles compared to traditional methods. In addition to the green synthesis method, The study has two key contribution. The first contribution is to synthesize new nanoparticles with antibacterial potential that can address the growing concern of bacterial resistance to existing antibiotics. The second contribution is to introduce new nanoparticles with antioxidant activity that can combat free radicals in the human body.

The importance of this study lies in its potential practical applications. The synthesized nanoparticles have extended antimicrobial and antioxidant activity, making them useful for a variety of applications such as biomedical, environmental, and industrial fields. The research also provides a valuable reference for further examination of metallic oxide nanoparticles and their potential applications in various fields. Overall, This study is significant in its contribution to the development of a more sustainable and effective approach to synthesizing nanoparticles while also addressing important issues such as bacterial resistance and free radical damage in the human body.

CHAPTER TWO

LITERATURE REVIEW

2.1 Metal and Metal Oxide Nanoparticles

Faraday identified the life of metal nanoparticles and Mie provided a quantitative explanation of their color. Metal-based nanoparticles are used in catalysis, sensing, and optoelectronics because their absorption sensitivity, and electrical, medicinal, magnetic, and catalytic properties depend on length, shape, and shape. Copper, zinc, gold, magnesium, silver, and titanium nanoparticles are of particular importance because of their antibacterial effect against *Bacillus subtilis and Staphylococcus aureus,* their use in medicine, dental care, water care, sunscreen creams, and coatings. Recently, metallic, ceramic, siliceous, and polymeric nanoparticles have been synthesized and used in a variety of packaging. Their small size and large area have fueled their use of textile technology and increased their demand. (Din & Rehan, 2017).

Due to increasing demand, eco-friendly synthetic routes to other metal oxides using certain plant extracts have been reported. The majority of research has concentrated on developing copper oxide, zinc oxide, iron, titanium dioxide, cerium dioxide, and selenium-based nanoparticles owing to the variety of industrial applications. Metal oxides are unpredictable compounds compared to noble metal nanoparticles such as those of Ag, Au, Pd, and Pt. Therefore, metal oxides require high-temperature treatment such as annealing or calcination processes at 300 ℃, 400 °C, 600 ℃, and 900 °C to remove the oxygen molecules and generate crystalline nanoparticles(Md Ishak et al., 2019).

Copper and copper oxide Nanoparticles

Copper has good electrical conductivity, high thermal conductivity, and corrosion resistance finding applications in gas sensors and photovoltaic cells. Other abilities of Cu and CuO nanoparticles primarily include catalysis and some of the NPs have been tested for their antibacterial and antioxidant activities. The plant-synthesized CuO NPs exhibit good catalytic degradation of methylene blue, significant antioxidant activity, and significant antibacterial effects against gram-positive and gram-negative bacteria(Md Ishak et al., 2019).

Zinc and zinc oxide nanoparticles

Today, Zn is currently being used across different industries such as rubber, ceramics, concrete manufacturing, cosmetics, food, and others. With the rise of technology, the development of micro and nano sized Zn is feasible and this can further broaden its applications. Zn is a semiconductor material with a wide bandgap width (3.37 ev) and large excitation binding energy(Sharma et al., 2022). ZnO is a member of the–VI semiconductor group and is known for having a wide band gap and large binding energy, making it preferable for use in photovoltaic, photocatalytic, cosmetics, electrochemical, light-emitting diode, and antibacterial applications. The majority of the ZnO produced by plant extracts crystallizes as hexagonal wurtzite crystals, which are the most stable when subjected to everyday environmental factors. The literature states that ZnO NPs were successfully made from Citrus maxima (Pomelo) fruit juice and that they had hexagonal wurtzite structure particle sizes in the 10–20 nm range. The NPs demonstrated effective photocatalytic methylene blue degradation as well as effective antibacterial action against pathogens, and they were utilized to create an electrochemical sensor for trace dopamine detection(Md Ishak et al., 2019).

Silver and silver oxide Nanoparticles

Ag Nps is an attractive inorganic material due to its environmentally friendly nature, with numerous applications in fields such as photography, diagnostics, catalysis, biosensing, and as antimicrobial agents. In the realm of nanotechnology, developing reliable and eco-friendly procedures for synthesizing metallic nanoparticles is crucial. AgO NPs is typically used for optical detection to have a surface resonance effect. AgO NPs demonstrate a sharper and stronger Plasmon resonance peak than Gold NPs, as their Surface Plasmon resonance performance is higher in particle concentration than in bulk. AgO NPs have now improved sensitivity for applications such as surface-enhanced Raman or localised surface plasmone resonance(Sharif Mughal & Mona Hassan, 2022). Several studies have achieved the goal of green synthesis of silver nanoparticles using a simple method (Patil et al., 2015). Silver nanoparticles possess antimicrobial properties, making them suitable for various medical applications such as coated blood-collecting vessels, capsules, band-aids, and more. Animal cells are not affected by silver's toxicity, but bacteria and other microbes are such as *E-coli*,

Pseudomonas aeruginosa, and *Staphylococcus aureus*. Because of these properties, it is regarded as a safe and effective bactericidal metal.(Saranyaadevi et al., 2014).

2.2 Some of Metal Oxide Composite Nanoparticles

Metal oxide composite nanoparticles have gained significant attention in recent years due to their unique properties and potential applications. Some of the metal oxide composite nanoparticles synthesized using various methods include, CuO-ZnO, TiO2-ZnO, and ZnO-CdS, among others. These composite nanoparticles exhibit superior properties compared to their individual metal oxide counterparts, such as enhanced synergistic effects, increased stability, and improved biocompatibility, making them attractive candidates for various fields, including biomedicine, catalysis, energy storage, and environmental remediation. The synthesis and characterization of metal oxide composite nanoparticles offer a promising avenue towards the development of novel materials with tailored properties and functionalities.

2.2.1 Green Synthesis of CuO−ZnO Nanocomposite

To synthesize CuO-ZnO nanocomposites, many methods use different precursors and reagents. However, a green chemistry approach aims to use environmentally friendly, low-cost chemicals and zero-waste methods to reduce chemical waste. Plant extracts provide safe, green, and naturally available biomolecules, making them a promising alternative to harsh chemicals. The biomolecules contained in the extracts act as reducing and stabilizing agents affecting the properties and morphology of the resulting nanomaterials. The type of biomolecules present in the extract plays a crucial role in their interaction with metal ions. Previous studies have reported on the synthesis of CuO-ZnO nanocomposites using plant extracts such as Clerodendrum infortunatum, Melissa officinalis, Vaccinium arctostaphylos L., and Ginkgo biloba, highlighting their potential not only in nanomaterial synthesis but also in medicine(Bekru et al., 2022). The CuO-ZnO nanocomposite has the ability as an antibacterial against S. aureus as gram-positive and E. coli as Gram-negative bacteria.

2.2.2 Green Synthesis of ZnO-SnO2 Nanocomposite

According to the following literature, it has been experimentally confirmed that Viscum album extract has excellent antioxidant properties due to its abundant phenolic and flavonoid compounds. It uses the alcoholic Viscum album extract to synthesize the ZnO/SnO2 composite nanoparticles in an eco-friendly way. The synthesized nanoparticles (ZnO/SnO2) were then used to photodegrade three organic pollutants commonly found in wastewater streams. The outstanding photocatalytic activity of the ZnO-SnO2 nanoparticles compared to the pure oxides can be attributed to the coexistence of two semiconductors with different CB and VB energy levels. The ZnO and SnO2 nanoparticles are n-type semiconductors and the difference between the CB edge and the flat band potential is negligible. Therefore, the valence band edge of ZnO and SnO2 can be determined by adding the band gap energy to the value of the flat band potential.(Sayadi et al., 2022)

2.2.3 Green Synthesis of Co_3O_4-ZnO Nanocomposite

The Co_3O_4-ZnO nanocomposite prepared by Green's method has also been reported in the following literature. However, the synthesis of green and plant extracts for various applications is still required to improve the catalytic efficiency. It is also known that much attention is paid to the green synthesis method of catalysts and the resulting materials are used in various applications. In particular, the eco-friendly synthesis of nanomaterials had several advantages: the method is non-toxic, easy to scale up, inexpensive, and environmentally friendly. For example, plant extracts could play an important role in the synthesis of metal nanoparticles with the required morphology and size, acting as natural reducing, encapsulating, and stabilizing agents. In addition, highly porous materials with high dispersion and specific surface area can be generated by using plant extracts as a template for catalyst synthesis. This phenomenon will help improve the catalyst activities of the materials and facilitate charge transfer. Researchers also used various plant extracts to boost the photocatalytic activities of semiconductors(Aragaw et al., 2020).

2.3 Types of Metal oxide composite Nanoparticles

a) Crown Jewel Structure: In this type of design, a single metal atom, known as the "jewel atom," is precisely arranged on the surface of another metal. The "diamond" metal is usually an expensive material that possesses catalytic capabilities, such as Au, Ag, or Pt.

b) Hollow Structure: These nanoparticles have a large pore volume and high surface-to-volume ratio, making them useful in non-reactor applications.

c) Heterostructure: One metal grows branches over another's nanocrystalline form.

d) Core-Shell Structure: This is a simple design in which one metal acts as the active shell and the other metal serves as the core. Core-shell bimetallic nanoparticles show promise as efficient catalysts.(Domènech et al., 2016).

In addition to the above-mentioned types, there are two more types of bimetallic nanoparticles:

e) Alloyed Structure: Bimetallic alloys are formed when two different metal atoms are uniformly distributed within a single particle.

f) Porous Structure: These bimetallic alloys have increased surface area, low density, and high gas permeability, making them superior catalysts compared to their solid counterparts.(Prakash et al., 2022)

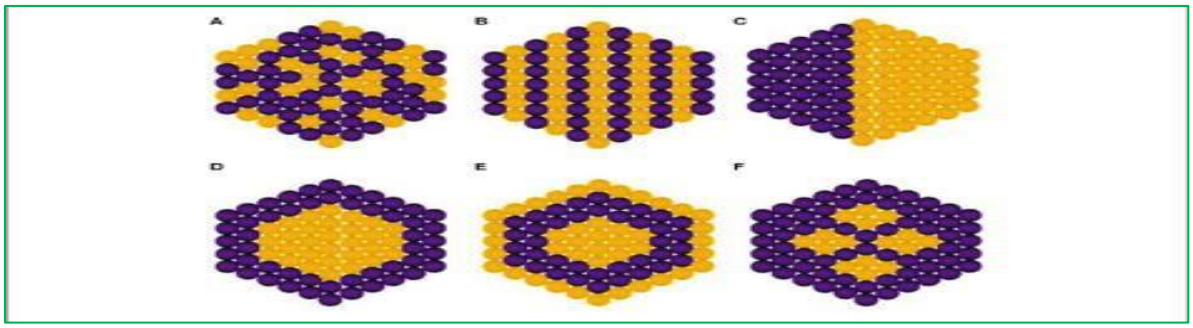

Figure 2: Types of bimetallic nanoparticles: (a) alloyed, (b) intermetallic, (c) sub-clusters, (d) core-shell, (e) multi-shell core-shell, and (f) multiple core materials coated by a single shell material.

2.4 Properties of Composite nanoparticles

The properties of composite metal oxide nanoparticles can differ significantly from those of elemental mono-metal oxide nanoparticles. Some of these properties are discussed below:

Catalytic properties

The incorporation of different metal nanoparticles results in the creation of bimetallic nanoparticles that possess superior catalytic properties. These properties have significant advantages for both scientific and technological advancements. A case in point is the combination of equal atomic concentrations of gold and silver nanoparticles, which is utilized in numerous catalytic reactions owing to their amplified surface area and reduced density(Loza et al., 2020).

Optical properties

The interaction between nanoparticles results in plasmatic coupling, which gives rise to intriguing optical properties. The excited surface electrons exhibit a distinct absorption pattern that imparts color to the nanoparticle dispersion. The absorption wavelength of surface plasmon resonance (SPR) is contingent on the constituent elements. In bimetallic nanoparticles, SPR discloses the internal distribution of elements, providing insight into their structure and properties. (Loza et al., 2020).

Antibacterial properties

The primary feature of nanoparticles is their ability to infiltrate cells and discharge bioactive ions. Gold-silver bimetallic nanoparticles display exceptional antibacterial activity against pathogenic bacteria, making them highly effective in combatting bacterial infections, such as *Staphylococcus aureus* and *Klebsiella pneumonia* (Nasrabadi et al., 2016).

Thermal conductivity

Nanoliquids, composed of bimetallic silver-gold nanoparticles in water, increase the thermal conductivity of liquids(Loza et al., 2020).

2.5 Chemistry of *Moringa stenopetala*

Moringa stenopetala is a member of the 14 kinds of Moringa, belonging to its own family Moringaceae. The plant is native to southern Ethiopia, northern Kenya, and Somalia. Commonly referred to as shiferaw in Amharic and cabbage tree in English, the plant has different names such as shelagda, halako, and aleko in numerous areas of southern Ethiopia. *M. stenopetala* is a versatile plant with particularly drought-resistant characteristics (Shumi, 2019).

The Moringa species that are native to Kenya are *M. stenopetala*, *M. arborea*, *M. borziana*, *M. rivae, and M. longitude*, of which *M. stenopetala* has drawn the most attention from researchers since it is widely used in traditional medicine(Ebenezar Udofia et al., 2020). In southern Ethiopia, people use the leaf for human consumption and animals. The plant has significant usage in traditional Ethiopian and Kenyan medicine as a remedy for various numbers such as diabetes, high blood pressure, stomach pain, malaria, leishmaniasis, leprosy, epilepsy, diarrhea, asthma, and the common cold, as well as as an anthelmintic, emetic and wound healing.

Some of these therapeutic claims for the different parts of the plant have been validated by pharmacological studies, including assessment of antimicrobial, antihypertensive, antispasmodic, and blood sugar, as well as other biochemical parameters. Today, the most extensive commercial use of Ethiopian moringa as a dietary supplement and medicine is through the consumption of dried leaves as an herbal tea(Habtemariam & Varghese, 2015).

A study by Habtemariam did look into the active principles responsible for the Ethiopian Moringa's potential usage as an antioxidant and treatment for diabetes and associated diseases. The powder of dried leaves has been extensively utilized as a natural medication and is broadly available in supermarkets in Ethiopia(Habtemariam & Varghese, 2015).

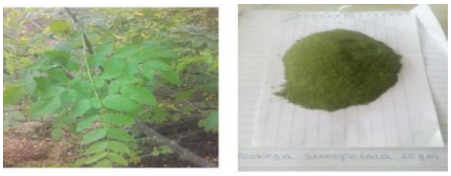

Figure 3: Moringa stenopetala, leaf (A), powder (B).

2.6 Methods for the Synthesis of Composite nanoparticles

In general, there are two methods for preparing nanoparticles: bottom-up (by reducing the metal cations) and top-down (by dissecting larger objects, e.g. by laser ablation or grinding) (Wagener et al., 2016). We'll look at them later. The bottom-up method requires a suitable soluble metal source, usually metal cations in the kind of soluble salts or coordinated by suitable ligands. A reducing agent is added to such a solution, the nature of which has a strong influence on the particle properties. Because the underlying processes of nucleation and crystal growth of a complex are still poorly understood(Xia et al., 2017).

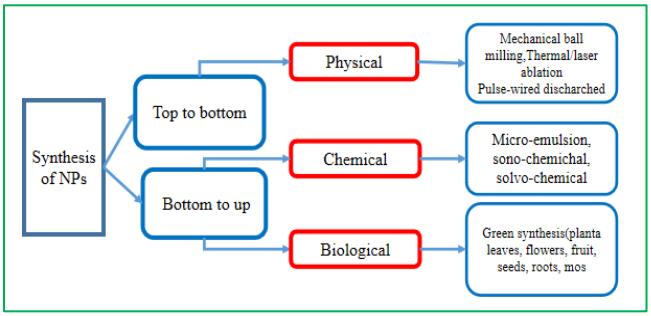

Figure 4: Top-down and bottom-up approaches using various physical, chemical, and biological methods to synthesize NPs.

The synthesis of bimetallic nanoparticles requires the utilization of a minimum of two distinct metal sources(e.g. Ag+ and Au3+) (Guisbiers et al., 2016). The nature of bimetallic nanoparticles is determined by the presence of both metal sources during reduction. If both metal precursors are present simultaneously, they may lead to alloyed nanoparticles where both metals (such as Ag and Au) are randomly mixed. In contrast, sequential reduction, which involves nucleus growth, can lead to the formation of core-shell particles(Sun & Xia, 2003).

The opposite situation is not always conceivable. Let's say Ag+ is first converted to silver nanoparticles, and then Au3+ is added. In this case, the more noble gold's cations oxidize metallic silver and deposit on the surface of the silver nanoparticle that is dissolving. This procedure has the potential to produce hollow gold nanoparticles with completely dissolved silver cores(Fu et al., 2016).

Laser ablation is considered the most controllable top-down method for synthesizing bimetallic nanoparticles. This involves directing a laser beam at a fixed target, such as a bimetallic alloy, under suitable conditions to obtain well-dispersed nanoparticles. These nanoparticles can then be subjected to further fractionation and surface-functionalization. Another alternative is a two-step synthesis, which involves exposing a mixture of silver and gold nanoparticles to laser irradiation(Loza et al., 2020).

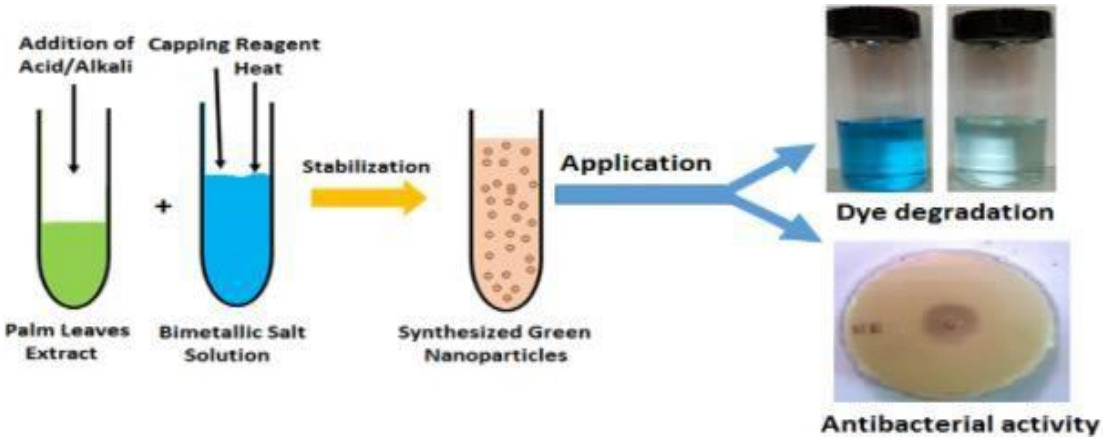

Figure 5: Schematic representation for the synthesis of bimetallic nanoparticles(Al-Haddad et al., 2020).

The typical procedure for synthesizing bimetallic nanoparticles using plant-mediated bottom-up approaches involves sequential reduction, which can induce the formation of core-shell nanoparticles. For instance, a metal salt can be reduced through the use of a plant extract, followed by the addition of a second metal ion, resulting in the formation of a core-shell bimetallic nanoparticle. The formation of such nanoparticles can be conveniently monitored by observing spectral changes within the UV-visible range, which arise due to the development of plasmonic absorption bands(Loza et al., 2020).

Core-shell nanoparticles are a prevalent type of composite nanoparticles owing to the integrated functionalities of the core and the coating. The physical and chemical properties of nanostructured composites, including optical properties, magnetic behavior, and chemical reactivity, can be adjusted by modifying the synthesis conditions in conjunction with the thermodynamic parameters(Chatterjee et al., 2014).

The synthesis of bimetallic nanoparticles by bottom-up approaches usually involves dissolving inorganic salts, such as silver nitrate and chloroauric acid, in water, followed by the addition of a plant extract. The mixture is continuously stirred at room temperature. When both metal precursors are added simultaneously, their reduction can occur simultaneously, leading to the formation of alloy nanoparticles(e.g. AuAg-BNPs)(Loza et al., 2020).

2.6.1 Green synthesis using plant extracts

Plants are utilized for the fabrication of metallic nanoparticles due to their abundance, cost-effectiveness, eco-friendliness, and non-toxic by-products. Green synthesis methods are straightforward, affordable, and non-hazardous to the environment. In chemical synthesis, the resulting products are unstable and require the use of stabilizing and protective agents, which are often toxic and expensive. Currently, there is a demand for simple, accessible, and scalable methods for obtaining nanoparticles at a reduced cost.

In the process of synthesizing metallic nanoparticles, phytochemicals serve two purposes: (1) as reducing agents and (2) as stabilizing agents for the nanoparticles(Yadi et al., 2018). Bimetallic nanoparticles synthesized through plant-mediated methods tend to be more stable and exhibit greater diversity in terms of shape and size. As such, the reducing agent found within the plant extract, such as flavonoids, terpenoids, and phenolic acid, plays a crucial role in the synthesis of bimetallic nanoparticles(Behzad et al., 2021). The diverse applications of bimetallic nanoparticles synthesized through plant-mediated methods are largely dependent on the synergistic effects of the metal ions present within them.

Bacteria-Mediated Synthesis of Nanoparticles

Gold nanoparticles were synthesized using the bacterium Delftia acidovorans, which is known to produce a small non-ribosomal peptide called delftibactin. This peptide has been associated with the synthesis of gold nanoparticles as it can induce resistance to toxic gold ions. The transition metal gold did not exhibit any toxicity in the vicinity of the bacterium, owing to the formation of inert gold nanoparticles that are active against delftibactin. Even novice products can function as stabilizers and reducing agents for the synthesis of gold nanoparticles, and these preparations demonstrate potential applications in medicine(Amal & Mohamad, 2013).

Biosynthesis of nanoparticles using fungi:

Fungi can secrete larger amounts of proteins, which convert directly into a larger amount of nanoparticles, and they posses a high binding potential with metal ions, so fungi can synthesize larger nanoparticles than bacteria. With strong substrate fermentation, they develop and cultivate without any problems. Using Fusarium oxysporum, extraordinarily stable silver hydrosols are synthesized, the debris of which has been stabilized using the proteins secreted via the fungus (Ahmad et al., 2003).

Biosynthesis of nanoparticles using algae:

In the plant kingdom, algae represent a diverse group of organisms that are being studied for their potential applications in the field of nanotechnology. Chlorella Vulgaris, for instance, has been utilized for synthesizing nanoparticles at ambient temperature. Seaweeds such as Caulerpa paresmosa, Sargassum polycystin, and Chaetomorpha linum have also been investigated for their ability to synthesize silver nanoparticles(Vijaylaxmee e al., 2014).

2.6.2 Factors Influencing Biosynthesis of Metal Oxide Nanoparticles

To synthesis nanoparticles with the correct size, shape, and quality for the intended use, the synthesis of nanoparticles requires the optimization of some parameters. The pH, temperature, reaction time, and metal ion concentration are the main variables affecting the biogenesis of nanoparticles. Successful nanoparticle synthesis depends on the reaction mixture's ideal temperature, pH, and metal ion concentration(Subbiah & Beedu, 2018).

Centrifugation of the nanoparticle solutions can be utilized to obtain pure bimetallic nanoparticles and prevent the interaction of multiple compounds, such as organic dyes, that may be used in analytical methods. Centrifugation at a speed of 10,000-15,000 rpm for 15-20 minutes can effectively isolate the nanoparticles and disperse them in distilled water(Thangaswamy et al., 2021).

The pH of the solution

pH is a critical experimental parameter that influences the growth dynamics of nanoparticles. This is because pH can have an impact on most of the equilibria involved in the nanoparticle

synthesis process(Mounika et al., 2010). The surface charge of nanoparticles can be reduced to zero at a particular pH, which is known as the isoelectric point (IEP). Numerous studies have demonstrated that pH plays a crucial role in regulating the size and formation of nanoparticles synthesized through various methods(Behzad et al., 2021).

In one study, the synthesis of Ag-Au bimetallic nanoparticles was completed within minutes of initiating the synthesis at pH 10. On the other hand, when AuAg bimetallic nanoparticles were synthesized through the co-reduction method, the reactants displayed two peaks (at around 500-550 nm and 400-420 nm) at pH 4-6, whereas at pH 7, the reactants exhibited a single peak at approximately 490 nm. These observations indicate that pH can have a significant impact on the formation and properties of bimetallic nanoparticles(Ganaie et al., 2016). The proposed optimal condition was pH 7(Akilandaeaswari & Muthu, 2021).

Reaction Temperature

Temperature is a critical physical parameter that can significantly affect the spatial and dimensional distribution of nanoparticles especially, Au–Ag BNPs, Ag–Pt BNPs, and Au–Pd BNPs (Dsouza et al., 2021). Experimental determinations using the proposed procedures are aimed at optimizing the experimental parameters involved in the biosynthesis process under investigation while taking into account the changes in the UV-VIS spectrum(Akinsiku et al., 2018). Analysis has shown that an increase in temperature results in an increase in the reaction rate during nanoparticle synthesis.

Higher temperatures favor the rapid conversion of the metallic solution into nanoparticles, whereas the synthesis process takes longer at room temperature(Roopan & Surendra, 2014). An increase in temperature raises the kinetic energy of the reactants, resulting in an acceleration of the nanoparticle synthesis process. This is because the elevated temperature can catalyze the formation of nanoparticles by promoting the formation of nucleation centers through the rapid reduction of metal cations(McClements & Öztürk, 2022).

Furthermore, high temperatures can result in the formation of smaller and more stable nanoparticles. It has also been reported that the absorbance of nanoparticles increases with temperature, indicating a higher concentration of synthesized nanoparticles. However, it is

important to note that the temperature must be maintained within the range of 30-100 ◦C, as phytochemicals can decompose at higher temperatures, potentially interfering with the reduction process and negatively affecting the quality of the synthesized nanoparticles(Akinsiku et al., 2018).

Reaction Time

The biosynthesis time is a crucial factor to consider during nanoparticle synthesis, as the reduction reaction cannot occur instantaneously, regardless of the extract used. It has been observed that the color transformation during bimetallic nanoparticle biosynthesis is dependent on the time and temperature at which the process occurs(Khodamorady et al., 2020). Au-Ag-BNPs were synthesized by adding 250 mL of 1 mM HAuCl4 + 250 mL of 1 mM AgNO3 in 100 mL of aqueous extract and heating the solution with stirring at 80-85 °C for 1 hour. The reaction process was monitored by UV-VIS spectroscopy for different time intervals.

Ag NPs formed after 90 minutes with an absorption at around 420 nm, while Au NPs formed after 60 minutes with an absorption at around 550 nm. The intensity of the band increased over time. The absorbance was observed at about 534 nm after 30 minutes and turned red at 542 nm after 45 minutes. Thus, increasing the reaction time increases the ion reduction rate until the reaction reaches completion.

Metal Ion Concentration

The initial concentration of metal ions in the reaction mixture is another critical factor that can significantly impact the synthesis of nanoparticles. For instance, in one study, AgSe bimetallic nanoparticles were synthesized using various concentrations of quercetin and gallic acid as reductants and coating agents. The researchers employed different dilutions of quercetin and gallic acid to investigate their effects on the synthesis process and the properties of the resulting nanoparticles (10-1,000 L) from the stock solution (10 mM) prepared in water and further diluted to 100 mL with deionized water to produce a reducing solution of different concentrations. An increase in the yield of AgSe NPs was observed when the metal salt concentration increased from 0.5 mM to 1 mM (Mittal et al., 2014).

Plant Extract/Biomass Dosage

The selection of the plant extract used for nanoparticle synthesis is influenced by several factors, including the plant species, the solvent used for extraction (with water being the most common), and the extraction temperature. These factors can affect the composition and concentration of the phytochemicals present within the extract, which in turn can impact the reduction and stabilization processes involved in nanoparticle synthesis(Khodamorady et al., 2020). Each plant has peculiarities in the phytochemical composition that affect the obtaining of different NP sizes.(Gopinath et al., 2016).

For instance, in one study, it was observed that increasing the concentration of reducing agents in Lawsonia inermis seed extract increased the intensity of the absorbers, suggesting that the synthesized nanoparticles were smaller and spherical. This highlights the importance of carefully controlling the concentration of reducing agents during nanoparticle synthesis to achieve the desired properties(Akilandaeaswari & Muthu, 2021).

Similarly, in another study, the intensity of absorbers in the UV-VIS spectrum increased with the concentration of pomegranate extract (Punica granatum) used as a reducing agent during nanoparticle synthesis. This observation suggests that the concentration of the reducing agent can significantly impact the properties of the synthesized nanoparticles, such as their size, shape, and stability(Ravikumar et al., 2019).

2.6.3 Phytochemicals In the Plant Extracts and Their Applications

Phytochemical investigations of plant extract in polar solvents like water and methanol showed that plants like Eichhornia crassipes possess secondary metabolites primarily Alkaloids, Phenolic groups, and Flavonoids which have anti-bacterial, anti-oxidant as well as nanoparticle stabilizing property. Alkaloids are nitrogen-containing alkaline, neutral, or weakly acidic compounds naturally found in plants. They have several sub-groups including chalcones, flavones, flavonols, and isoflavones with unique major sources (Panchal & Parvez, 2019). Flavonoids are considered to be a crucial component in the synthesis of MNP and MONPs. The basis for flavonols is the presence of the benzene ring(Narayana et al., 2001). (Love et al., 2015).

In addition to providing protection against ROS generated during photosynthesis and exposure to man-made pollutants, phenolic chemicals also protect plants. Because they are phenol derivatives with at least one carboxyl functional group, phenolic acids are believed to have powerful antioxidant properties and are widely used in medicine. Most phenolic acids also contain other chemical and structural components, including larger polyphenols. The hydroxyl groups of these structures can scavenge ROS and free radicals(Gallon et al., 1994).

Phenolic chemicals are abundant secondary metabolites found in medicinal plants. Several plant-based meals and syrups contain phytochemical phenolic acid, which is widely known for its anti-inflammatory, anti-cancer, and antioxidant activities.(Kassim et al., 2010). By using phenolic acids as a reducing agent, one can prepare MNPs using a thermodynamic equilibrium approach. Nucleation is started by injecting the reducing agent (phenolic acids) at the concentration where metal ions are supersaturated, and the MNPs' subsequent growth is achieved through progressive ion reduction. (Shafey, 2020).

Polyphenols and terpenoids are known to play both reducing and/or stabilizing agent roles. Plant extracts rich in saponins, tannins, glycosides, and phytosterol can aid in the creation of nanoparticles of small size(Raja et al., 2017). A class of phenolic chemicals known as flavonoids can scavenge free radicals and oxidative enzymes, resulting in analgesic and anti-inflammatory effects. These mixtures are considered both antioxidant chemicals and phenolic compounds. In other words, combinations of phenols and flavonoids, found in varying amounts in different parts of the plant, are partially responsible for the antioxidant effects of plants.

Many studies have shown that phytochemicals such as phenols, flavonoids, and carotenoids are at the root of the antioxidant, antibacterial, and antifungal effects of plants. Scientists in various fields of applied sciences have become interested in the formation and study of NPs in the last few decades(Azizian-Shermeh et al., 2020).

2.7 Green Synthesis of CuO Nanoparticles

Copper oxide nanoparticles have been synthesized on a large scale using various plant extracts in an herbal manufacturing process. In this process, the metal salt is mixed with the plant extract, and the reaction takes place at room temperature for 1-3 hours. The plant extract generates

electrons that reduce copper salts, resulting in the formation of copper oxide nanoparticles when phytochemicals react with copper ions. (Chakraborty et al., 2022).

2.7.1 Green synthesis of Co_3O_4 nanoparticles

Cobalt oxide (Co_3O_4) NPs have been extensively exploited due to their unique and wide range of applications(Bibi et al., 2017). Using natural plants to synthesize cobalt nanoparticles is an economical, environmentally friendly, and convenient process compared to other physical or chemical methods. Plants are enriched with various essential phytochemicals, which can act as reducing, closing, and stabilizing agents, reducing the need for additional chemicals.

The powdered plant material is then mixed with a solvent to extract the phytochemicals, which are subsequently used as reducing agents for cobalt salt solutions. The mixture is then subjected to various process parameters such as temperature, pH, and reaction time to facilitate the reduction process and the formation of cobalt nanoparticles. The final step involves separating the nanoparticles from the reaction mixture and characterizing them using various analytical techniques(Singh, 2022). Therefore, we used this facility to synthesize Co_3O_4 NPs and investigated their multifunctional applications. Furthermore, previous reports have shown that Co_3O_4 NPs were prepared using different protocols and their antibacterial potential was investigated on gram-negative and gram-positive bacterial species(Bekele et al., 2022).

2.7.2 Green synthesis of Copper-cobalt oxide composite nanoparticles

In a recent study, copper oxide/cobalt oxide composite nanoparticle were synthesized using an environmentally friendly and cost-effective method involving Moringa stenopetala leaf extract. The plant extract was prepared and characterized using various analytical techniques, including UV-visible spectrophotometry and Fourier transform infrared spectrometry. These techniques were used to study the optical and chemical properties of the synthesized nanoparticles. The resulting bimetallic nanoparticles were found to have potential applications in various fields, including catalysis and energy storage. This study highlights the potential of plant-mediated nanoparticle synthesis as a green and sustainable approach to nanomaterial production.(Shehu et al., 2020).

Nanoparticles have a wide range of applications both in the biomedical and physical-chemical fields. In the biomedical field, they can be used for drug delivery, biosensing, bioimaging, and biomolecular recognition. Due to their antimicrobial properties, nanoparticles are incorporated into various materials of daily use, including cosmetics, toothpaste, deodorants, water purification systems, and humidifiers. In agriculture, nanoparticles play an important role in detecting and controlling plant diseases and minimizing nutrient leaching to increase crop yields. They can be used as fertilizers, pesticides, and herbicides, and can also improve the overall health and growth of plants.

Nanoparticles are also used in solar and oxide batteries for energy storage. They can be used as catalysts in chemical reactions for various industrial processes, and the development of new materials with unique properties. Additionally, they have potential applications in environmental remediation, such as the removal of pollutants from soil and water. Overall, the versatility and unique properties of nanoparticles make them valuable tools in a variety of fields and applications, with the potential for even more exciting applications in the future. (Zhang et al., 2020).

2.7.3 Applications of Biosynthesized Metal Oxide Nanoparticles

Antioxidant Activity

Phytochemicals can be found in various parts of the plant, including just under the bark or in the outer leaves. They are specific to each plant and even each plant cell. Some authors suggest that phytochemicals, along with precious metal content in nanoparticles, may reduce the risk of lung, breast, or colon cancer.

The antioxidants present in plants are responsible for the green synthesis of metal nanoparticles or metal oxides due to their ability to reduce or chelate metal ions and act as stabilizers for the produced nanoparticles. The use of plant extracts as reducing and stabilizing agents for nanoparticle synthesis represents a green and sustainable approach to nanomaterial production, with significant potential for various applications in biomedicine, agriculture, and energy storage (Martinello & Mutinelli, 2021).

Antibacterial Activity

Bimetallic nanoparticles, such as Cu-Ni and Fe-Ag, have shown promising antibacterial and antifungal activity against certain strains of bacteria and fungi. Cu-Ni nanoparticles have demonstrated a bacteriostatic effect against Escherichia coli, Staphylococcus aureus, and Staphylococcus mutants, while Fe-Ag nanoparticles have shown excellent antifungal and antibacterial activity against pathogenic microorganisms.

The use of bimetallic nanoparticles in nanomedicine represents a promising approach to combatting infectious diseases and addressing the growing problem of antibiotic resistance. However, further research is needed to fully understand the mechanisms of action of these nanoparticles and their potential toxicity in vivo(Prakash et al., 2022).

Anticancer Activity

Bimetallic iron-based nanoparticles have the potential to enhance cancer treatment by improving cancer cells. Bimetallic nanoparticles that contain gold and silver are utilized both in vitro and in vivo for the photothermal healing of many types of cancers.(Valodkar et al., 2011). Cancer is a malignant disease in which atypical cells multiply uncontrollably and can invade the surrounding healthy tissue.

Certain cells come from every tissue in the human body and can be found anywhere in the body. The BNPs act as chemotherapeutic agents in the treatment of tumor cells and show a synergistic effect with drug chemotherapy. Many studies show that BNPs have anti-cancer hobbies(Ghosh et al., 2015). BNPs have been reported to have a cytotoxic effect on numerous types of cancer cells, including most breast cancer cell lines.(Burlacu et al., 2020).

Antidiabetic Activity

Diabetes is a metabolic disease that causes excess glucose in the blood (hyperglycemia) and is manifested by a lack of insulin secretion or insulin resistance. Diabetes is the third leading cause of death worldwide after cardiovascular disease and cancer(Burlacu et al., 2020). Glucosidase and amylase enzymes (porcine) are considered important antidiabetic enzymes that metabolize carbohydrates. It mediates the cleavage of polysaccharides and disaccharides to glucose.

Therefore, the use of inhibitory glucosidase delays the digestion and absorption of carbohydrates(Lebovitz, 1997). Synthesized BNPs, such as Au–Ag BNPs and Pt–Pd BNPs, using various plant resources, show antidiabetic activity.

2.7.4 Anti-bacterial action of CuO nanoparticles

The use of copper-containing nanoparticles (NPs) has been demonstrated to be effective against animal and plant pathogens by preventing the formation of multi-drug resistant (MDR) biofilms. These NPs have the potential to serve as antimicrobial coating agents. Copper NPs can inhibit the growth of MDR bacteria, and their antimicrobial activity is similar to that of silver NPs but at a lower cost.

Copper oxide NPs can generate reactive oxygen species (ROS), leading to chromosomal DNA degradation. This effect appears to be due to a specific effect of the particles rather than the release of metal ions. Researchers have studied the effects of CuO NPs on bacterial denitrification and explored their impact on the expression of intracellular proteins.(Baptista et al., 2018).

2.7.5 Anti-bacterial action cobalt oxide nanoparticles

Eltarahony et al. reported the green synthesis of combined Co NPs using gram-negative bacteria *P. mirabilis*. The characterization of NPs was confirmed by UV-Vis, SEM, XRD, TGA dynamic light scattering (DLS), and polydispersity index (PDI). The antibacterial activity was observed using a good diffusion assay against *S. typhiea, E. coli, C. perfringens, S. aureus*, and *Enterococcus faecalis*. The result showed that the NPs show promising biocidal efficacy against these bacteria (Eltarahony et al., 2018). Green-mediated cobalt oxide NPs were synthesized using *Hibiscus rosa-sinensis* flower extract and their antibacterial activity was measured. Therefore, at minimal concentrations, cobalt oxide nanoparticles can be an effective antibacterial agent(Iravani & Varma, 2020).

2.7.6 Antioxidant Activity

An essential component of nanoscience and nanotechnology is the assessment of the antioxidant activity of nanomaterials. Free radicals are created during both healthy and unhealthy cellular

metabolism, but an excessive amount of oxygen-derived free radicals can cause several diseases to manifest. Antioxidants are essential for defending biological systems from damaging events such as excessive oxidation, protein damage, DNA damage, and cell death. Various kinds of natural and synthetic substances have been the subject of several studies looking at their antioxidant properties. An approach frequently used to investigate a material's antioxidant capabilities is the DPPH scavenging assay. (Dobrucka, 2018).

2.7.7 DPPH Assay

P. guajava leaf extracts' flavonoids and polyphenolic elements have antioxidant properties that shield cells from the oxidative stress brought on by free radicals. The prevention of the negative consequences of many diseases, including cancer, depends on free radical scavenging activities. The DPPH test has historically been used to evaluate plant extracts' antioxidant capacities. The reason antioxidants have an impact on DPPH is thought to be their capacity to donate hydrogen. Depending on the concentration, the chemicals are diluted into a purple DPPH solution and turn yellow(Govindasamy et al., 2022a).

CHAPTER THREE

MATERIALS AND METHODS

In this chapter, the study site, materials, and methods of the experiment were presented. The first part of the chapter covered the study site, various chemicals, samples, and instruments required to carry out this research and in the second section of this chapter, synthesis methods of samples for CuO Nps, Co_3O_4 Nps, and CuO-Co_3O_4 Composite Nps, some characterization methods and finally the method to test the antibacterial and antioxidant activity of the prepared nanoparticles were presented.

3.1 Study Area Description

The Green synthesis of CuO NPs, Co_3O_4 NPS, and CuO-Co_3O_4 nanocomposite using *moringa stenopetala* plant extract was carried out in Applied Chemistry Department Laboratory, Adama Science and Technology University and the XRD and TGA analysis of the synthesized nanoparticles were performed in Materials Science Department laboratory, Adama Science and Technology University. The SEM micro image was performed at Adama Science and Technology University in the Applied Biology department laboratory. UV-Vis spectroscopy analysis of the synthesized nanoparticles was performed at Addis Ababa Science and Technology University (AASTU). FT-IR analysis was performed at Bahir Dar University. The antioxidant activity test of the synthesized nanoparticles was carried out in Applied Chemistry Department Laboratory which is located at Adama Science and Technology University. Finally, the anti-bacterial activity tests of the synthesized nanoparticles were carried out at Adama public health referral and research laboratory center.

3.2 Chemicals and Reagents

In this study, Trihydrate copper nitrate (Cu $(NO_3)_2.3H_2O$, 99.8%), Dimethyl sulfoxide (DMSO), Sodium hydroxide (NaOH, Sigma aldria 99% purity), Cobalt (II) nitrate hexahydrate ($CoNO_3.6H_2O$, 99.9%,), Ferric chloride (Sigma aldria, 99%, purity), chloroform, sulfuric acid(H_2SO_4, Sigma aldria 98% purity), Ethanol (C_2H_5OH 99.8%, Ethiopia), Distilled water. 2, 2-Diphenyl-1-picrylhydrazyl hydrate (DPPH) was used. All reagents were analytical grade and

purchased from Addis Abeba, Ethiopia (YESHADAM TRADING PLC, PARACHEM INDUSTRY & TRADING PLC, and ET WISDOM IMPORT & EXPORT PLC) Local market and used without further purification.

3.3 Instruments and Apparatus

Magnetic stirrer, Aluminium foil, volumetric flask, centrifuge, crucible beakers, measuring cylinders, analytical digital balance, burette, dropper, spatula, conical flasks, filter paper (Whatman No-1), Oven, Furnace, Refrigerator, Water bath, Mortar, and pestle were used. The instruments that were used for characterizing the synthesized NPs include UV-Vis spectroscopy (UV3600plus, SHIMADZU, Japan), which helped us to study the optical properties of the nanoparticles and nanocomposite, FT-IR (FTIR Perkin Elmer's spectrophotometer), for analysis of the vibrational modes of atoms in the molecules, PXRD (SHIMADZU, XRD-7000S, Japan), to characterize the nature of crystal structure of nanoparticles, SEM (JCM-6000plus BENCH TOP SEM, SHIMADZU Corporation, Japan), was used to study the morphology of the synthesized nanoparticles, and TGA (Differential Thermal gravimetry), DTG-60H, SHIMADZU Corporation, Japan).

3.4 Synthesize Procedures

3.4.1 Preparation of *Moringa Stenopetala* Leaf Extract

The *Moringa stepenotala* leaves were collected from Adama Science and Technology University campus, Oromia regional state, Ethiopia. The leaves were washed repeatedly with running tap water and rinsed with de-ionized water. The leaves were air-dried for 6 days. The samples were cut into small units and ground with the aid of mortar and pestle. About 10 g of the dry leaf sample was weighed and soaked in 200 mL of de-ionized water and boiled at 80 ^{o}C on a hot plate with frequent stirring for 30 min. The extract was cooled and filtered with Whatman no. 1 filter paper. The aqueous extracts were stored in a sealed plastic container at 20°C (Shehu et al., 2020).

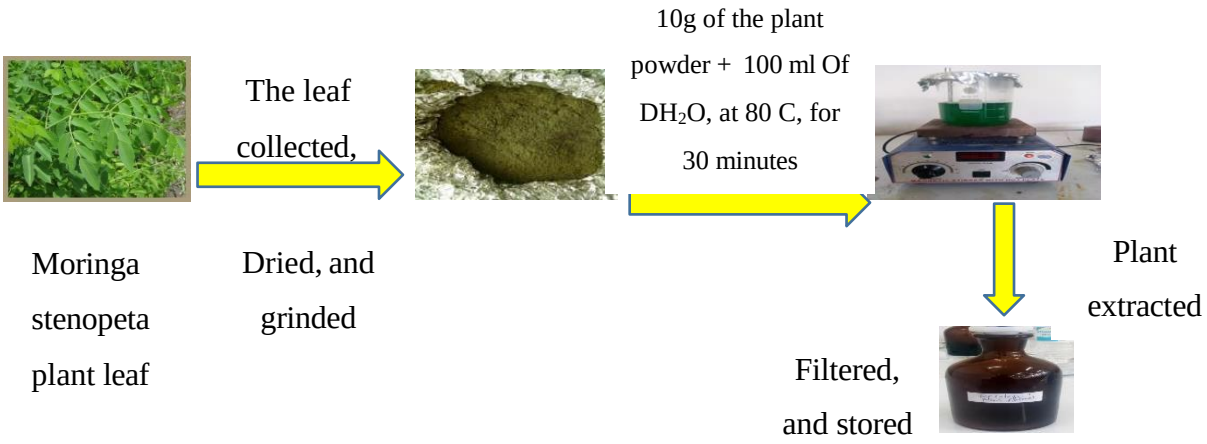

Figure 6: General procedure for aqueous extract of *Moringa stenopetala* plant leaf

3.4.2 Phytochemical Analysis of Aqueous Extract Moringa Stenopetala Plant

The plant extract was subjected to assessment for the existence of the phytochemicals by using the following reported standard methods(Panchal & Parvez, 2019).

Tests for Flavonoids (Alkaline Reagent Test): 2 mL of 2.0% NaOH mixture was mixed with aqueous plant crude extract; a concentrated yellow color was produced, which become colorless when 2 drops of diluted acid were added to the mixture. That result showed the presence of flavonoids.

Test for tannins (Ferric chloride test): 2 mL Plant extract was taken in the test tube and boiled. 5 drops of 0.1% $FeCl_3$ were added and gave a brownish-green or a blue-black color, which confirmed the presence of tannins.

Test for terpenoids (Salkowski test): 2 mL of aqueous plant extract was been mixed with 2 mL of chloroform and 3 mL concentrated H_2SO_4 carefully to form a layer. A reddish-brown coloration of the interface was formed and shows positive results for the presence of terpenoids.

Test for Steroids: 2 mL of chloroform and concentrated H_2SO_4 were added with the 5 mL aqueous plant crude extract. In the lower chloroform layer, the red color has appeared that indicating the presence of steroids.

Tests for Glycosides (Salkowski's Test): 2 mL concentrated H_2SO_4 was added to the aqueous plant extract.

A reddish-brown color was formed which indicates the presence of steroidal aglycone part of the glycosides.

Test for phytosterols (Salkowski's test): 2 mL of aqueous plant extract and 10 mL of chloroform were added and then filtered. 5 drops of concentrated H_2SO_4 were added to the filtrate; the mixture was shaken and examined for the appearance of a golden yellow color.

Test for saponins: 0.5 g of plant extract was taken, then 5 mL of distilled water was added and shaken while heating to boil. Frothing was shown in the presence of saponins.

Test for phenols: 5 drops of 2% of $FeCl_3$ were added to 2 mL of aqueous plant extract and the formation of a bluish-green to black color indicates the presence of phenols.

3.4.3 Procedure for Synthesis of CuO Nanoparticles

The synthesis of CuO nanoparticles was conducted with a precipitation method (Andualem et al., 2020)(Benhammada & Trache, 2022). In a typical procedure, a stoichiometric amount of 0.2 mol L^{-1} Cu $(NO_3)_2.3H_2O$ was dissolved in 500 mL of distilled water under magnetic stirring; then, 100 mL of *moringa stenopetala* plant aqueous extract was added to 100 mL of the metal salt solution, and the mixture was heated under stirring at 80 °C for 30 min. The solution color was changed from blue to brown-green. At that temperature, the aqueous solution of NaOH (2 mol L^{-1}) was introduced dropwise until pH = 11, and the precipitate was observed. The precipitate of the sample *was*, then, centrifuged at 1000 rpm for 20 min and washed with deionized water and ethanol to remove impurities. Finally, the precipitate was dried in an oven at 150°C for 3(1/2) hrs and was ground to a fine powder using an agate mortar. the black powder obtained from the above-mentioned method was calcinated.

Figure 7: General procedure for the biosynthesis of copper oxide nanoparticles using *Moringa stenopetala* extract

3.4.4 Procedure for Synthesis of Co_3O_4 Nanoparticles

For the fabrication of cobalt oxide NPs, freshly prepared plant extract (100 mL) was added to 0.2 M solution (100 mL) of $Co(NO_3)_2.6H_2O$, and this reaction solution was kept on the hot plate for 3 hr at 80 °C to synthesize cobalt oxide nanoparticle. After 3 hr, the solution was transferred into the oven at 100 °C for 5 hr to get the dried precipitate. Further, the precipitate of cobalt oxide NPs was calcinated. Finally, synthesized Co_3O_4 NPs were characterized by spectroscopic and microscopic analysis(Govindasamy et al., 2022a)

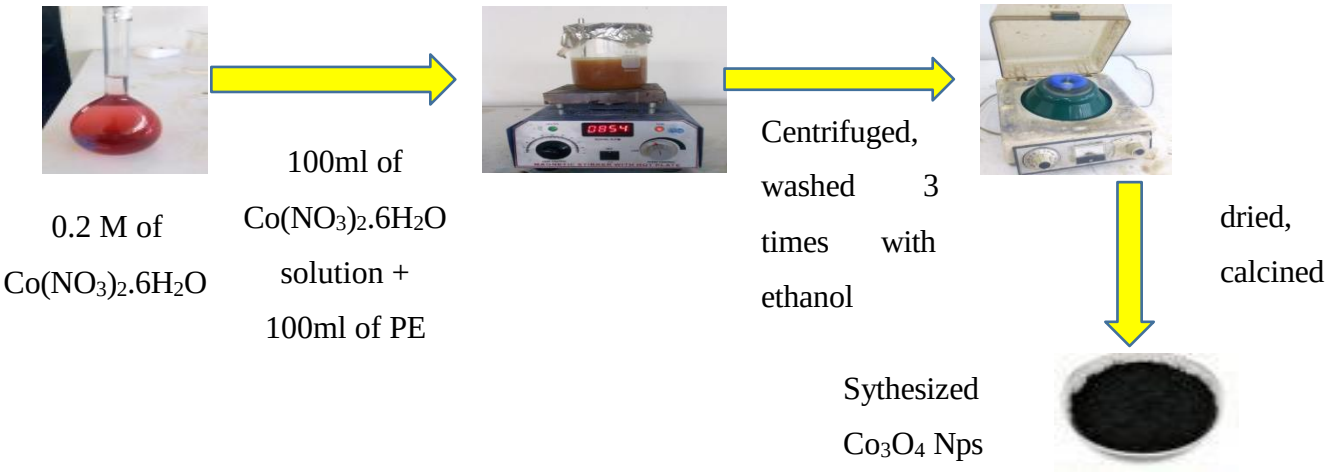

Figure 8: General procedure for the biosynthesis of cobalt oxide nanoparticles using Moringa stenopetala extract

3.4.5 Procedure for Synthesis of CuO-Co_3O_4 Composite Nanoparticles

Synthesis of CuO-Co_3O_4 Composite NPs using *moringa stenopetala* leaf extract was carried out according to the literature mentioned below with minor modifications. For the synthesis of CuO-Co_3O_4 Composite NPs, 100 mL of 0.2 M $Cu(NO_3)_2.3H_2O$ solution was added to the 1000 mL beaker. Then, 100 mL of 0.2M $Co(NO_3)_2.6H_2O$ solution was added to the beaker while stirring for 15 min. After 15 min 200 mL of plant, extract was added to the solution slowly while heating at 60 °C for 5 h with constant stirring. Then the mixture was settled at room temperature for 24 hr, and the solution was centrifuged for 20 min at 2000 rpm. Then, the solid part was washed with distilled water and ethanol then dried on a ceramic crucible for 24 h at 70 °C in the oven.

Finally, the powder obtained was calcinated and then was kept for further analysis(Aragaw et al., 2020).

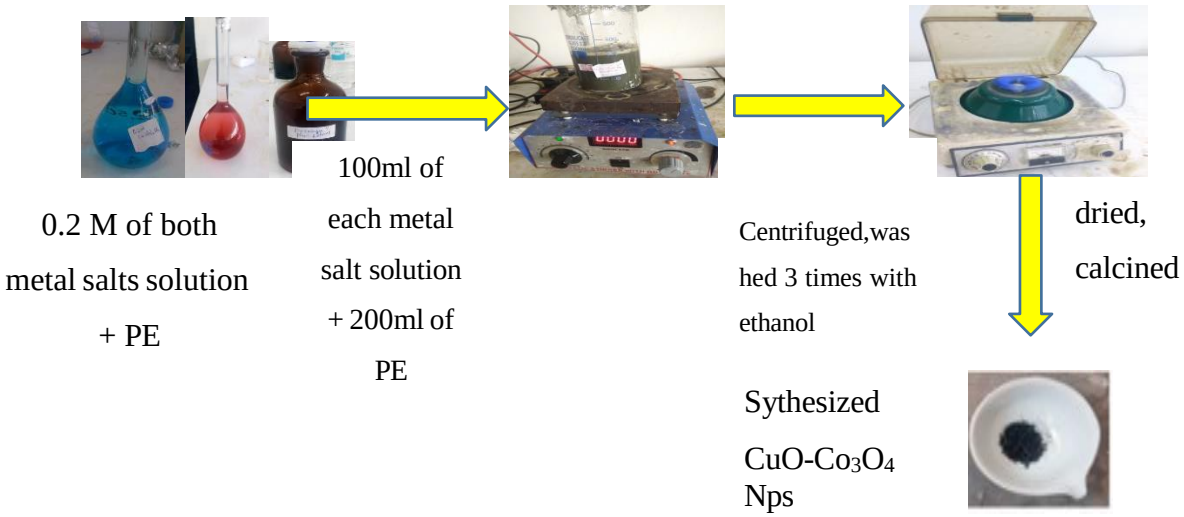

Figure 9: General procedure for the biosynthesis of copper oxide-cobalt oxide nanoparticles using Moringa stenopetala extract.

3.5 Characterization of CuO Nps, Co_3O_4, & CuO-Co_3O_4 Composite Nps

3.5.1 UV-Vis Spectroscopy Analysis

The optical properties of biosynthesized CuO Nps, Co_3O_4, and CuO-Co_3O_4 Composite nanoparticles were characterized by a UV-Vis spectrophotometer. The range of absorption was between 200 nm to 800 nm. In the parabolic band structure, the band gap energy, Eg, and the absorption coefficient of a direct band gap semiconductor are related through Equation (1):

$$(\alpha hv)2 = A(hv - Eg) \qquad (1)$$

Where ħ is Planck's constant, v is the photon's frequency, and is the slope in the linear region. Taking the K–M scattering coefficient S as a constant concerning the wavelength, and using the remission function in Equation (1), the following expression was derived from Equation (2):

$$(F(R)hv)2 = A(hv - Eg) \qquad (2)$$

Where, F(R) is equal to K/S, the molar absorption coefficient K is equal to (1 – R)2, the scattering factor S is equal to 2R, and R is the reflectance of the materials and is defined as $\frac{\%R}{100}$. The direct and indirect bandgap energies of the nanomaterials were determined by extrapolation of the linear portion of Kubelka–Munk (K–M) plots (Abebe et al., 2021).

3.5.2 Powder X-ray diffractometer (PXRD) Analysis

To determine crystallinity, structure imperfections, and crystallite size of the synthesized CuO Nps, Co_3O_4, and CuO-Co_3O_4 Composite Nps, XRD were examined by using the Shimadzu XRD-700 Powder X-ray diffractometer (PXRD). The x-ray diffraction (PXRD) patterns were recorded at the range of 2θ from $2\theta = 10° \leq 2\theta \leq 80°$ with a scan rate of 20/ min using Cu Kα radiation with an accelerating voltage of 40 KV. The crystallite size D of a particle can be estimated according to the Scherrer equation:

$$D = \frac{K\lambda}{\beta \cos\theta} \qquad (3)$$

Here, the x-ray wavelength λ is 0.154 nm, k is the structure factor, which is assigned a value of 0.94, D is the average diameter of the crystals, θ is the Bragg angle in degrees, and β is the full-width at half-height of the prominent peaks.

Sample Preparation: 1-2 grams of dried CuO Nps, Co_3O_4, and CuO-Co_3O_4 Composite Nps ground by mortar and paste, and then it was filled into the sample holder and subjected to Powder X-ray diffractometer.

3.5.3 Scanning Electron Microscop(SEM) Analysis

SEM analysis of the biosynthesized CuO Nps, Co_3O_4 Nps, and CuO-Co_3O_4 Composite NPs was carried out by using SEM (JCM-6000 plus BENCH TOP SEM, SHIMADZU Corporation, Japan) which reveals information about the external morphology of the biosynthesized CuO Nps, Co_3O_4, and CuO-Co_3O_4 Composite Nps with direct visualization.

3.5.4 Fourier Transform Infrared (FTIR) Analysis

FTIR analysis of the synthesized nanoparticles were conducted accordingly. FTIR spectrum of the dried powder of the biosynthesized CuO Nps, Co_3O_4 Nps, and CuO-Co_3O_4 Composite NPs

samples was recorded on FT-IR in the range 4000-400 cm^{-1}. FT-IR is used to identify the functional groups of the active components responsible for synthesizing CuO Nps, Co_3O_4 Nps, and CuO-Co_3O_4 Composite NPs.

3.5.5 Thermogravimetric analysis (TGA) Analysis

Thermogravimetric analysis of the biosynthesized CuO Nps, and Co_3O_4 Nps were done in a flowing air atmosphere and the thermograms were recorded in the temperature range of 25–800 ^{0}C, at a heating rate of 20 ^{0}C/min. TGA measures the percent weight loss of a test sample.

Sample Preparation: A piece of powder specimen (6–7 mg) was placed in a platinum basket, and a thermocouple beneath the basket continually monitored the temperature. TGA calculates the percent weight loss of a test sample while it was heated evenly in the proper atmosphere.

3.6 Procedure for Antibacterial Activity Test

The synthesized CuO NPs, Co_3O_4 NPs, and CuO-Co_3O_4 Composite NPs were screened for *in vitro* antibacterial activities against four bacteria strains (*Escherichia-coli (*Gram-negative), *Staphylococcus aureus* (Gram-positive), *Streptococcus pyogenes* (Gram-positive), and *P aurus* (Gram-negative)) by Agar disc diffusion method (Linh et al., 2018). The bacterial stock cultures were maintained on the sheep blood agar slants at 37 ^{o}C. Freshly, grown liquid culture of the test strains having similar turbidity with 0.5 McFarland was seed over the Mueller Hinton agar medium with a sterile swab.

The disc measuring 6 mm in diameter were prepared from Whatman filter paper and sterilized by dry heat at 121 ^{o}C for 20 min. The different concentrations of CuO NPs, Co_3O_4 NPs, and CuO-Co_3O_4 nanocomposite (24, 12, 6, and, 3 mg/mL) were prepared by dissolving synthesize nanoparticles in DMSO. Then, sterilize 6 mm filter paper discs and soak them in each prepared nanoparticle. The growth inhibition zone were measure in mm after 24 hr incubation at 37 ^{o}C and compared with the standard drug Gentamicin. DMSO was used as a negative control and 25 µg Gentamicin was used as a standard drug. All the above procedures will be repeated three times and the mean standard deviation of a zone of inhibition were taken(Gopinath et al., 2016).

3.7 Measurement of antioxidant activity by DPPH scavenging assay

The DPPH scavenging assay was considered an easy as well as cost-effective well-known method for the determination of the antioxidant activity of materials since the radical is stable at room temperature. To study the antioxidant capacity, 1 mL of 10 mg/mL, 20 mg/mL, 30 mg/mL and, 40 mg/mL of each CuO NPs, Co_3O_4 NPs and, CuO-Co_3O_4 Composite nanoparticles were added separately to 1 mL of 0.2 mM Methanolic DPPH solution (by dissolving 3mg of DPPH in 50 mL of methanol), which was added to four different test tubes. The reaction mixture was incubated at room temperature for 30 min. Then the absorbance was recorded at 517 nm using a Shimadzu UV-2550 UV-Visible spectrophotometer. The color of the DPPH solution eventually turned colorless or pale yellow as the reaction progressed due to the antioxidant activity of the produced nanoparticles. Antioxidant activity (%) of the synthesized nanoparticles was estimated using the following mathematical relation.

$$\textbf{\% of DPPH scavenging} = \left[\frac{Ac - As}{Ac}\right] \times 100 \quad (4)$$

Where, Ac is the UV-Visible peak intensity at 517 nm for control (DPPH) and As is the UV-Visible peak intensity at 517 nm for the supernatant DPPH solution(Das & Saikia, 2022).

Statistical analysis

All experiments were done in triplicates and obtained results were represented as mean±standard deviation (SD). SD was present in graphs as error bars. Origin Pro software was used to perform all the statistical analyses.

CHAPTER FOUR

RESULTS AND DISCUSSION

This chapter begins by presenting the results of the phytochemical screening of *Moringa stenopetala* plant extract. In the following section, UV-Vis absorption spectra and calculated band gaps of the synthesized NPs are presented. Then the X-ray diffraction results are examined, covering crystal size, lattice parameters, microstrains, and dislocation densities of CuO, Co_3O_4, and CuO-Co_3O_4 composite nanoparticles. The fourth section of this chapter deals with the SEM analysis, while the fifth section briefly outlines the functional groups and their assignments of the synthesized NPs. The sixth section of this chapter deals with the TGA analysis. Finally, in the last section, the antibacterial and antioxidant activities of the synthesized nanoparticles are discussed.

4.1 The Phytochemical Screening Test Results

Phytochemical screening of extracted *Moringa stenopetala* plant extracts was carried out to understand the phytochemicals responsible for the reduction and/or capping of the metal oxides during nanoparticle synthesis. Therefore, the results of the phytochemical analysis of *Moringa stenopetala* plant extracts are summarized in Table 1 and supported by Figure 10.

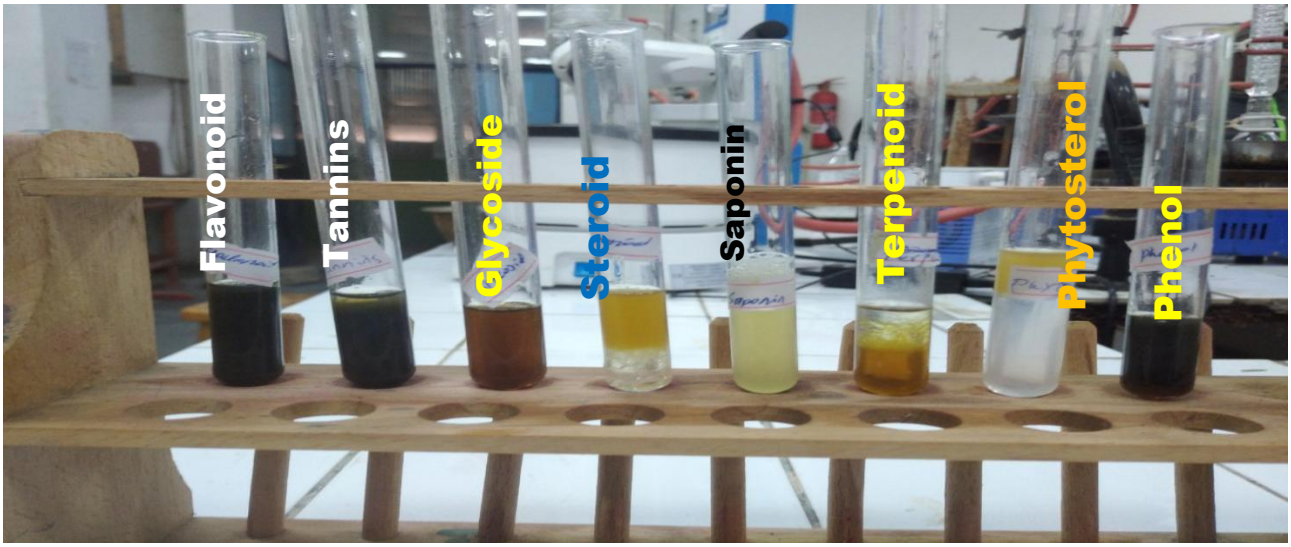

Figure 10: Results of phytochemical screening of Moringa stenopetala plant extract.

Table 1: Results of phytochemical screening of *Moringa stenopetala* plant extract

S. no	Secondary Metabolite	Results
1	Flavonoids	+
2	Tannins	+
3	Terpenoid	+
4	Steroid	+
5	Glycosides	+
6	Phytosterols	-
7	Saponins	+
8	Phenols	+

The results gathered showed that the main phytochemical components of the *Moringa stenopetala* plant extract were flavonoids, tannins, terpenoids, steroids, glycosides, saponins, and phenols, which are supposed to be responsible for aiding in the synthesis of CuO, Co_3O_4, and CuO-Co_3O_4 composite nanoparticles.

4.2. UV- Vis spectroscopy analysis Results

The optical properties of the biosynthesized CuO NPs, Co_3O_4 NPs, and CuO-Co_3O_4 composite NPs are shown as follows. Figure 11 (a and b) shows the absorption spectra and energy band gap for CuO NPs. Figure 12 (a and b) shows the absorption spectra and energy band gap for Co_3O_4 NPs and similarly, Figure 13 (a and b) presents the absorption spectra and energy band gap for CuO-Co_3O_4 composite NPs. In the UV-Vis spectrum of the synthesized CuO NPs, the surface plasmon absorption of metal oxide resulted in an absorption peak at 263 nm as shown in Figure 11(a), No additional peaks were found in the 200-800 nm range and the absorption peak was found to be symmetrical.

The surface plasmon absorption in the metal oxide nanoparticles is based on the collective oscillation of the free conduction band electrons excited by the incident electromagnetic radiation. This type of resonance occurs when the wavelength of the incident light far exceeds the particle diameter. The surface plasmon absorption band with a maximum of 263 nm indicates the formation of CuO nanoparticles(Naika et al., 2018).

This result obtained agrees with the reported literature value, for CuO NPs, the surface plasmon resonance is in the range of 200–350nm(Akintelu et al., 2020). The results were also in good agreement with the cited study(Shelke et al., 2022). The bandgap energy for the synthesized CuO NPs was determined by the Tauc relations and the plots were shown in figure 11 (b), which indicates the band gap of synthesized CuO Nps is 3.32 eV.

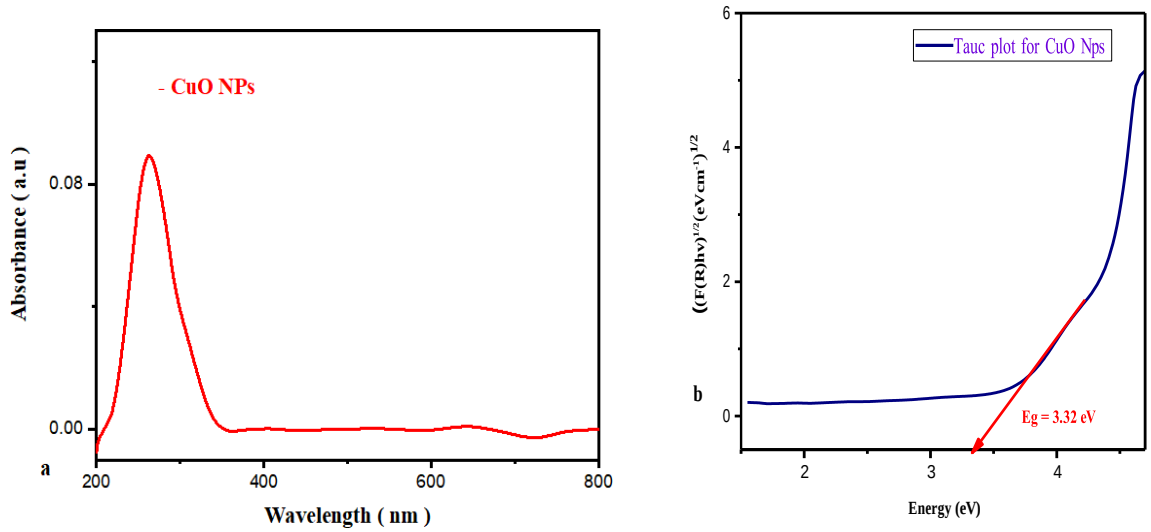

Figure 11: (a) Wavelength versus Absorbance of UV-Vis spectroscopy, (b) energy versus band gap of CuO NPs.

The absorption spectra and energy band gap of Co_3O_4 NPs and CuO-Co_3O_4 composite NPs are shown in Figure 12(a and b) and, Figure 13(a and b) respectively.

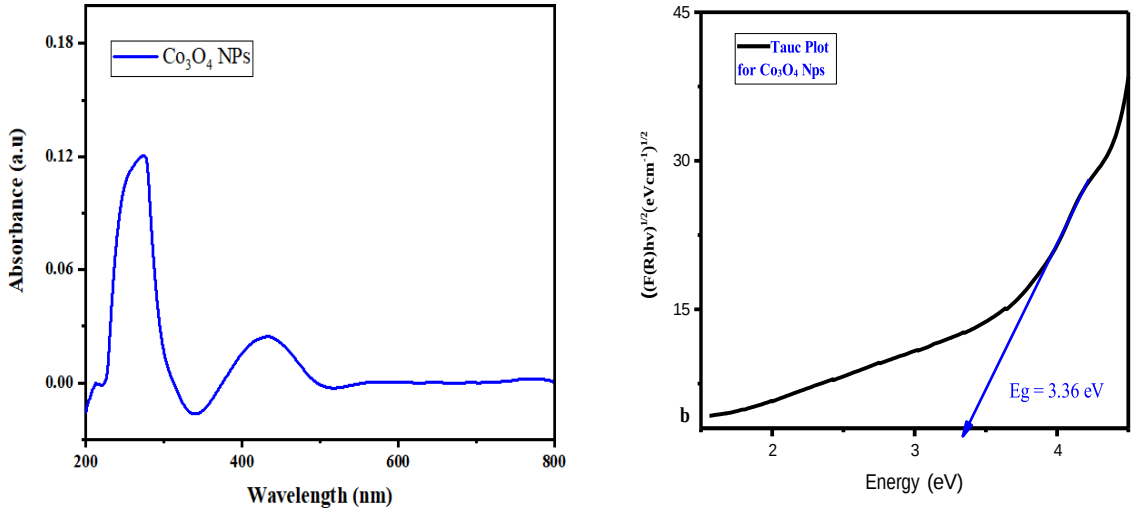

Figure 12: (a) Wavelength versus Absorbance of UV-Vis spectroscopy, (b) energy versus band gap of Co_3O_4 NPs.

The absorbance and bandgap spectra of phyto-mediated Co_3O_4 nanoparticles are displayed in Figure 14(a and b) with characteristic peaks corresponding to Co_3O_4 nanoparticles observed at around 280 nm and 441 nm. The first broad and the second slightly visible two peaks of Co_3O_4 nanoparticles elucidated the transition of charges from O to Co orbitals. Co^{2+} and Co^{3+} orbital electrons move towards the O^{2-}, which indicates the double oxidation state of cobalt elements.

Phyto-mediated Co_3O_4 nanoparticle's calculated band gap is 3.36 eV, which was well agreed with previously reported band gap for Co_3O_4 nanoparticles(Govindasamy et al., 2022b). The wide band gap of Co_3O_4 nanoparticles explained the gap between the holes and electrons, which suppressed the recombined activity. The obtained photo exciton charge carriers provoke the oxygen vacancy on the Co_3O_4 nanoparticles. The charge carrier mitigations and partings may deduce the organic pollutants and deactivate the bacterial system in wastewater and biomedical applications.

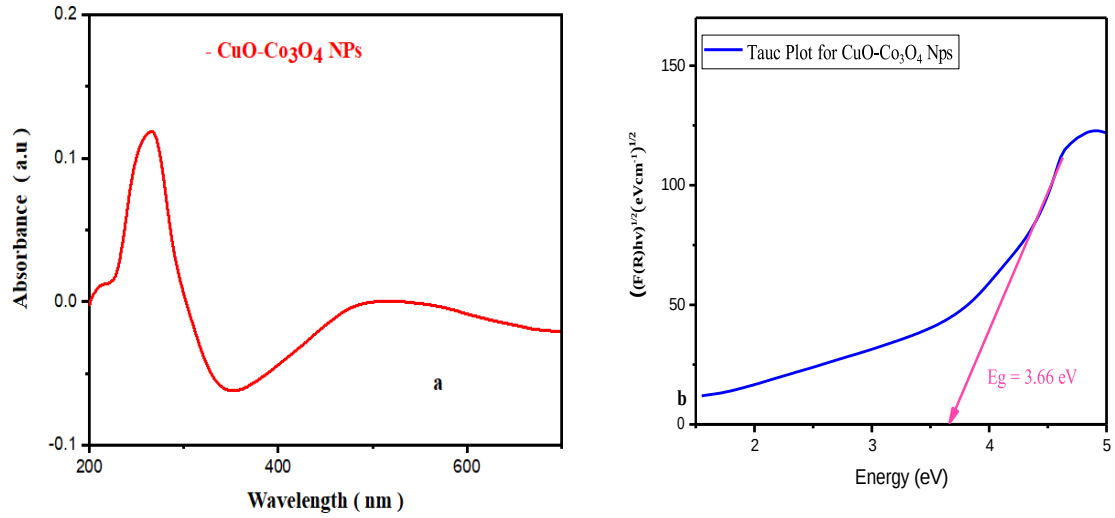

Figure 13: (a) Wavelength versus Absorbance of UV-Vis spectroscopy, (b) energy versus band the gap of $CuO\text{-}Co_3O_4$ composite NPs.

From Figure 15 (b) the optical energy band gap of $CuO\text{-}Co_3O_4$ composite NPs found to be 3.66 eV. The optical band gap increased on average in the final composite NPs relative to their monometallic counterpart. This indicates that the composite NPs exhibited strong quantum confinement, which shifts the energy levels of the conduction and valence bands apart and gives rise to a blue shift in the transition energy as the particle size decreases(Meghdadi et al., 2017)Das et al., 2013).

4.3 Powder X-ray diffraction (PXRD) Analysis Results

Powder XRD analysis was performed to analyze the structure and crystallinity of the synthesized CuO NPs, Co_3O_4 NPs, and $CuO\text{-}Co_3O_4$ composite NPs. Figure 14 shows the XRD results of the prepared samples. Experimentally obtained samples were identified by comparison to standard CuO NPs and Co_3O_4 NPs samples. For CuO NPs, diffraction peaks were observed values: 32.7°, 35.8°, 39.02°, 53.75°, 58.52°, 61.85°, 66.38°, 68.28°, 72.6°, and 75.38° which correspond to (110), (-111), (111), (200), (20-2), (002), (113), (220), (113), (311), and (004) planes as shown in Figure 15 (a). The spectral data showed that the synthesized CuO NPs exhibited a monoclinic phase, and the observed peaks were fitted using the Joint Committee on Powder Diffraction

Standard (JCPDS Map #048-1548), space group C2/c), which agrees with that previously reported work(Andualem et al., 2020).

The XRD pattern of Co_3O_4 NPs has been presented in Figure 14 (b), and in the diffractogram, the diffraction peaks were observed at 2θ = 18.99°, 31.31°, 36.88°, 38.43°, 44.86°, 55.69°, 59.42°, 65.30°, and 77.45° corresponding to the miller indices (hkl) values of (111), (220), (311), (222), (400), (422), (511), (440), and (533) respectively. The spectral data obtained showed that the synthesized Co_3O_4 NPs showed cubic spinel crystal structure phase and the observed peaks were fitted with the Joint Committee on Powder Diffraction Standard (JCPDS card No. 042-1467, space group Fd-3m), which is in agreement with the previously reported work (Govindasamy et al., 2022a).

The XRD diffraction pattern of CuO-Co_3O_4 composite NPs is presented in Figure 14 (c). The peaks at 2θ values 18.99°, 31.37°, 36.85°, 44.68°, 53.54°, 61.60°, 65.90°, 72.40°, 75.10°, and 77.51° corresponding to the miller indices (hkl) values of (111), (220), (311), (400), (200), (002), (440), (311), (004) and (533) respectively. The diffraction peaks at 2θ values of 53.54°, 61.60°, 72.40°, and 75.10° are associated with the (20-2), (113), (311) and (004) planes of monoclinic phase CuO (JCPDS card No. 48-1548), and the peaks at 2θ values 18.99°, 31.37°, 36.85°, 44.68°, 65.90°, and 77.51° correspond to the miller indices of (111), (220), (311), (400), (440), and (533) are planes of Co_3O_4 (JCPDS card No. 042-1467) confirming that the synthesized CuO-Co_3O_4 nanostructures have a crystalline structure.

It can be seen that both CuO and Co_3O_4 peaks can be found in the sample. The relative intensities of the Co_3O_4 peaks decreased compared to those of the CuO peaks due to the formation of the CuO shell coating on the Co_3O_4 core surface.

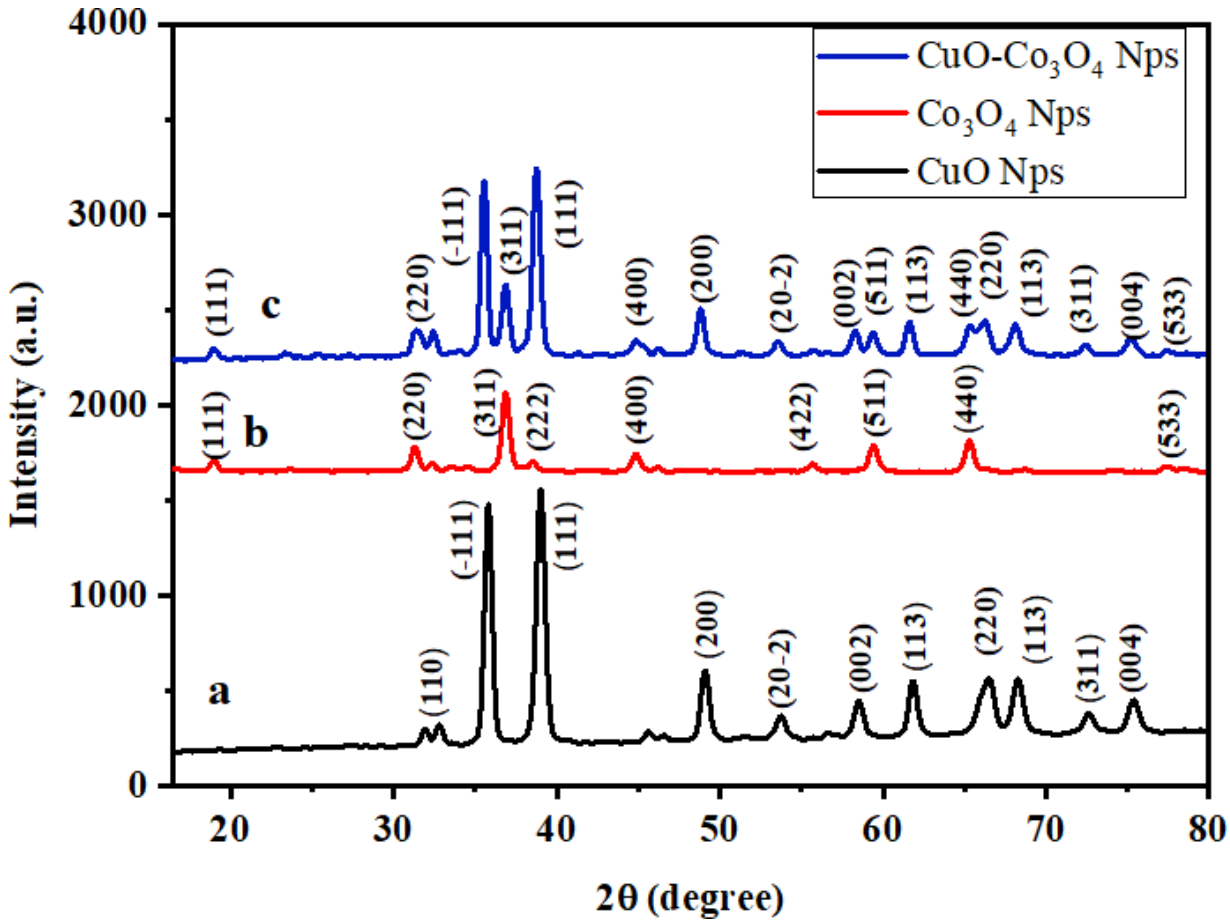

Figure 14: X-ray diffraction patterns a) CuO NPs, b) Co_3O_4 NPs, and c) CuO-Co_3O_4 composite NPs.

For the synthesized CuO NPs, Co_3O_4 NPs, and CuO-Co_3O_4 composite NPs the d-spacing (d), particle size (D), dislocation density (δ), and microstrain (ε) were calculated, and presented in the table (2-4) below for the strongest peaks of respective synthesized NPs.

Table 2: The calculated parameters for the strongest peaks of CuO NPs

No.	2θ	θ	β	D (nm)	D average (nm)	d- spacing	δ x 10^{-3}(nm^{-2})	ε x 10^{-3}
1	32.7	16.39	0.47	16.08	11.59	2.72	3.86	7.02
2	35.8	17.90	0.50	15.06		2.50	4.40	6.77
3	39.02	19.51	0.59	12.63		2.30	6.26	7.29
4	53.75	26.87	0.53	13.13		1.70	5.79	4.64
5	58.52	29.26	0.56	12.28		1.57	6.62	4.39
6	61.85	30.92	0.54	12.59		1.49	6.30	3.94
7	66.38	33.2	1.02	6.49		1.40	23.71	6.82
8	68.28	34.14	0.70	9.29		1.37	11.57	4.55
9	72.6	36.3	0.21	9.81		1.25	10.85	1.29
10	75.38	37.69	0.73	8.59		1.25	13.54	1.29

The average crystallite size of the CuO NPs was deduced to be 11.59 nm

Table 3: The calculated parameters for the strongest peaks of Co_3O_4 NPs

No.	2θ	θ	β	D(nm)	Daverage (nm)	d- spacing	δ x 10^{-3}(nm^{-2})	ε x 10^{-3}
1	18.99	9.49	0.49	15.73	12.25	4.66	4.04	13.0
2	31.31	15.65	0.52	14.49		2.85	4.76	8.21
3	36.88	18.44	0.55	13.58		2.43	5.41	7.25
4	38.43	19.21	0.93	8.06		2.34	15.37	11.64
5	44.86	22.43	0.60	12.20		2.01	6.71	6.36
6	55.69	27.84	0.53	13.16		1.64	5.76	4.40
7	59.42	29.71	0.62	11.01		1.55	8.23	4.78
8	65.30	32.65	0.61	10.89		1.42	8.42	4.18
9	77.45	38.72	0.55	11.17		1.23	8.00	3.01

The average crystallite size of the Co_3O_4 NPs was deduced to be 12.25 nm.

Table 4: The calculated parameters for the strongest peaks of CuO-Co_3O_4 NPs

No.	2θ	θ	β	D(nm)	D average (nm)	d- spacing	δ x 10^{-3} (nm^{-2})	ε x 10^{-3}
1	18.99	9.49	0.59	13.20	9.53	4.66	5.73	15.48
2	31.37	15.68	1.57	4.85		2.84	42.42	24.47
3	36.85	18.42	4.90	1.53		2.43	42.18	64.28
4	44.68	22.34	0.99	7.37		2.02	18.38	10.57
5	53.54	26.77	0.49	14.34		1.71	4.85	4.27
6	61.60	30.80	0.52	13.07		1.50	5.85	3.82
7	65.90	32.95	1.18	5.62		1.41	31.59	7.97
8	72.40	36.20	0.47	13.48		1.30	5.49	2.83
9	75.10	37.55	0.60	10.45		1.26	9.14	3.41
10	77.51	38.75	0.54	11.35		1.23	7.75	2.96

The average crystallite size of the CuO-Co_3O_4 NPs was deduced to be 9.53 nm

Based on the above calculation data, one can correlate the peak position (2θ), average crystal size (D) and microstrain (ε), and dislocation density (δ) as follows: The decrease in the microstrain (ε) shows that the angle (2θ) or peak position increased, the average crystal size increases with increasing peak position and this shows that crystal size also contributes to peak broadening. Dislocation density measures the number of dislocations in a unit volume of crystalline materials. With the increasing particle size of the nanoparticles, the dislocation density of the crystalline materials decreases.

In other words, as the peak position (angle) increases, the dislocation density of the crystalline particle decreases. The synthesized CuO NPs, Co_3O_4 NPs, and CuO-Co_3O_4 composite NPs have an average crystal size of 11.59 nm, 12.25 nm, and 9.53 nm, respectively. Peak positions (2) are

increased in these sequences. Since the dislocation density depends on the particle size, this means that as the particle size increases, the dislocation density decreases. Thus, the dislocation density decreases in the order CuO-Co_3O_4 composite NPs < CuO NPs < Co_3O_4 NPs.

4.4 Scanning Electron Microscopy (SEM) analysis Results

The morphology of the synthesized CuO NPs, Co_3O_4 NPs, and CuO-Co_3O_4 composite NPs are presented in SEM images and is shown in Figures 15(a), 15(b), and 15(c) respectively. The SEM image of the synthesized CuO NPs is shown in Figure 15(a). The synthesized CuO NPs exhibited heterogeneous composition. The SEM images show the presence of some large granular particles, which could be due to the aggregation or overlapping of smaller particles associated with the oxidation of nanoparticles. This fact agreed with reports that CuO NPs agglomerate into either clusters or large nanoparticles.(Krishna et al., 2020).

The SEM images of Co_3O_4 NPs are shown in Figure 15(b). The secondary metabolites and chemical components contained in *Moringa stenopetala* leaf extract affect particle agglomeration as bioactive molecules encapsulate and stabilize each particle. Larger particles are formed due to the reactivity and attraction of the functional groups. These particles are coated with hydroxyl groups on the surface of various biological substances. The component appears to be agglomerated due to the formation of hydrogen bonds with the molecules surrounded by these active ingredients(Govindasamy et al., 2022b).

It is clear from the SEM image that the components were non-uniformly and agglomerated. This improves the ability of the biosynthesized Co_3O_4 NPs to suppress microorganisms through their smooth surface. On the other hand, the Co_3O_4 nanoparticles had different size particles and irregular geometries, suggesting that they were well dispersed. The SEM image of CuO-Co_3O_4 composite NPs in Figure 15(c) also revealed the inhomogeneity of the particles in terms of their shape and size. The micrographs show that the CuO-Co_3O_4 composite NPs have both spherical and irregular geometries with different particle sizes in the micrographs.

a) 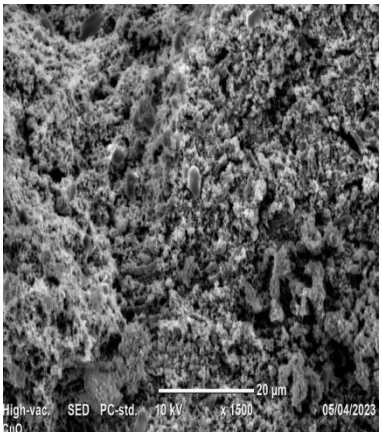

b) 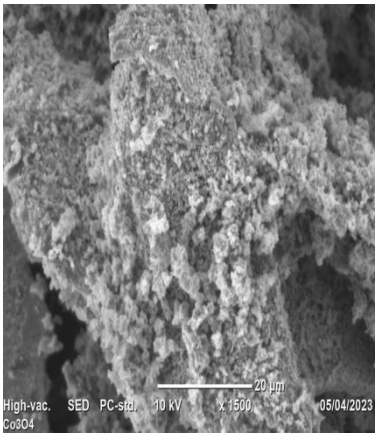

c) 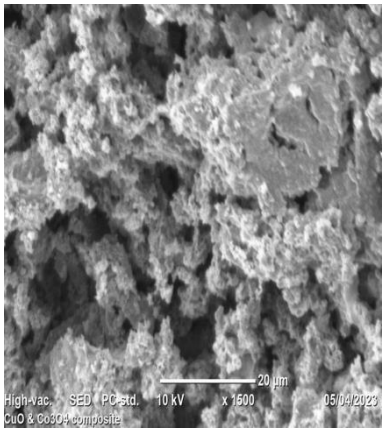

Figure 15: SEM image of (a) CuO NPs, (b) Co_3O_4 NPs, (c) CuO-Co_3O_4 Composite NPs

4.5 Fourier Transform Infrared (FT-IR) Spectroscopy Results

FTIR analysis of the green synthesized CuO NPs, Co_3O_4 NPs, and CuO-Co_3O_4 composite nanoparticles as well as the leaf extract of *Moringa stenopetala* was performed to reveal the formation of CuO NPs, Co_3O_4 NPs, and CuO-Co_3O_4 composite. The FTIR analysis is commonly used to study nanoparticles and confirm the function of groups present in the leaf extract of the Moringa stenopetala plant and new functional groups that might emerge in the nanoparticles and nanocomposites. This is used to confirm that the bioactive molecules were actively involved during the synthesis process as stabilizing and capping agents to prevent the overall growth of CuO NPs, Co_3O_4 NPs, and CuO-Co_3O_4 composite nanoparticles. Figure 16 shows the FT-IR result of *Moringa stenopetala* plant leaf extract and CuO NPs.

The FTIR spectrum for leaf extract of *Moringa stenopetala* plant figure 16 (a) showed the absorption bands at 3437 cm^{-1}, 2901 cm^{-1}, 1606 cm^{-1}, 1383 cm^{-1}, 1008 $cm^{-1,}$ and 572 cm^{-1}. The broad peak observed in the spectrum at around 3437 cm^{-1} confirms the presence of O-H stretching. While the absorption peak located at around 2901 cm^{-1} reveals the presence of C-H stretching vibrations of alkane. A peak at 1606 cm^{-1} showed the presence of carboxyl(C=O) stretch and the observed peak at 1383 cm^{-1} showed an N-H Bend of primary amines.

The absorptions peak around 1008 cm^{-1} C-O stretch of the ether functional group. The peak at 572 cm^{-1} may correspond to the presence of aryl disulfide (S–S) or Polysulfides (S–S stretch) or C–Br stretch(Dalvand et al., 2016).

Figure 16 (b), clearly indicates the peak shifts after the reaction of copper nitrate with leaf extract. The peak shifted, suggesting that the responsible functional groups were involved in the binding mechanism on the CuO NPs. The broad absorption band at 3388 cm^{-1} corresponds to the hydroxyl (OH) functional group in alcohols and phenolic compounds. The peak absorption at 2921 cm^{-1} corresponds to the C-H stretching of Alkane. The IR band around 1612 cm^{-1} can be assigned to the aromatic bending of the alkene group (C=C). The sharp peak at 1383 cm^{-1} is attributed to the deformation vibration of the C–H band of the alkane (CH_3 and CH_2) group. The absorption peak at 1008 cm^{-1} stretching vibration of the C–O group of primary and secondary alcohols (C–O). The peaks around 764, and 537 cm^{-1} correspond to the Cu–O stretching vibration of copper oxide nanoparticles in the monoclinic structure. (Varughese et al., 2020)(Varughese et al., 2020).

The FTIR spectrum of Co_3O_4 NPs and CuO-Co_3O_4 composite nanoparticles also showed some shifting in the peaks; peak intensity decreased/increased, and disappeared. Figure 18 showed the FT-IR results of Co_3O_4 NPs and CuO-Co_3O_4 composite Nanoparticles. The absorption peaks of Co_3O_4 NPs and CuO-Co_3O_4 composite nanoparticles were observed at 3423 cm^{-1}, 2913 cm^{-1}, 1612 cm^{-1}, 1413 cm^{-1}, 1006 cm^{-1}, 862 cm^{-1}, 648 cm^{-1}, 552 cm^{-1} and 3423 cm^{-1}, 2913 cm-1, 1612 cm^{-1}, 1358 cm^{-1}, 1006 cm^{-1}, 696 cm^{-1}, 559 cm^{-1} respectively.

Figure 17 (a) indicates the FT-IR spectra of the sample Co_3O_4 NPs exhibit, the absorption peak at 3423 cm^{-1} corresponding to –OH stretching of the carboxylic acid. The absorption peak located at around 2913 cm^{-1} reveals the presence of C-H stretching vibrations of alkane. The peaks located at 1612 cm^{-1} may be due to C=C stretching. The absorption peak revealed at 1413 cm^{-1} and 1006 cm^{-1} corresponds to the N=O Bend of the nitro group and C-O stretch of the ether functional group respectively. Moreover, the peaks at 659 cm^{-1} and 569 showed the stretching vibration of Co–O, corresponding to the tetrahedral and octahedral coordination of Co^{2+} and Co^{3+}, respectively.(Aragaw et al., 2020) (Diallo et al., 2015)(Bhargava et al., 2018).

Figure 17(b) shows FT-IR spectra of the sample CuO-Co_3O_4 composite nanoparticles exhibited, band at the band at 3423 cm^{-1} indicating the –OH stretching of the carboxylic acid. The band located at around 2913 cm^{-1} shows the presence of C-H stretching vibrations of alkane. The absorption peak around 1612 cm^{-1} and 1358 cm^{-1} indicated the N=O Stretch of the Nitro group and N=O bending of the nitro group. While the absorption peak at 1006 cm^{-1} indicated the presence of C-O stretch of the ether functional group. The peak at 696 cm^{-1} may correspond to the presence of substituted alkene. The absorption peak at 559 cm^{-1} corresponds to the stretch Co-O present in CuO-Co_3O_4 composite Nanoparticles(Das et al., 2013)(Bhargava et al., 2018)(Naika et al., 2018).

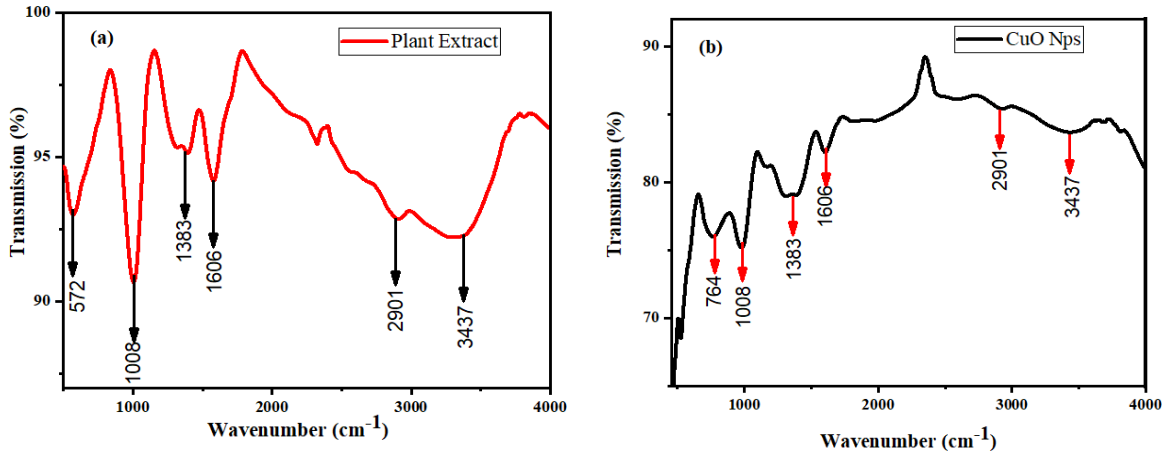

Figure 16: FTIR spectra of (a) Moringa stenopetala plant extract, (b) CuO NPs

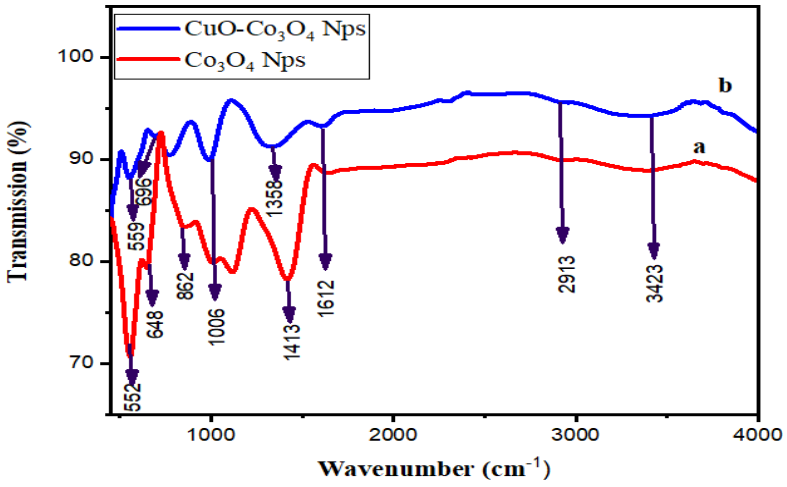

Figure 17: FTIR spectra of (a) Co_3O_4 Nps, (b) CuO-Co_3O_4 composite Nanoparticles

4.6 Thermogravimetric analysis (TGA/DTA) Results

The thermal behavior or thermal stability of biosynthesized CuO NPs and Co_3O_4 NPs that were capped by phytochemicals of *Moringa stenopetala* plant extract was investigated via thermogravimetric analysis. Thermogravimetric analysis was conducted under a nitrogen atmosphere at a heating rate of 10 ^{o} C/min. The green synthesized CuO NPs using copper nitrate trihydrate precursor salt and *Moringa stenopetala* leaves extract was characterized by using TGA/DTA.

The weight losses of the investigated materials were analyzed. Figure 19 (a) shows the thermal gravimetric analysis and differential thermal analysis of the bio-synthesized CuO NPs. The TGA curve shows the mass loss of the sample, whereas the DTA curve indicates the energy gain or loss during the process. As can be observed from Figure 19(a), the TGA curve of CuO NPs showed three-step decomposition and weight losses were observed in the temperature ranges of 188.75 ^{o}C– 402.5 ^{o}C, 402.5 ^{o}C–514.45 ^{o}C, and 515 ^{o}C– 600 ^{o}C.

The weight loss of the material observed in the temperature range of 188.75 ^{o}C – 402.5 ^{o}C was about 28.29%, and this was mainly due to the vaporization of water content from the sample. The sample also showed a weight loss of about 15.87% in the temperature range of 402.5 ^{o} C–514.45 ^{o}C which could be due to the combustion of biomolecules from the *Moringa stenopetala* extract that remained in the biosynthesized NPs. The weight loss observed in the temperature range of 515 ^{o} C–600 ^{o}C was about 30.56% which may be due to escaping of oxygen from the sample. In general, from TGA analysis, the total weight loss calculated was 75.33%, and the TGA results suggested that this compound is thermally stable(Andualem et al., 2020).

Figure 18 (b), shows the thermo gravimetric analysis and differential thermal analysis of the bio-synthesized Co_3O_4 NPs. For Co_3O_4 NPs weight loss of 49.07% was observed from room temperature to 340 ^{o} C. The first 33.45% could be due to the loss of residual ethanol or absorbed moisture. The second weight loss 15.62% could be due to the loss of oxygen, enhancing the formation of oxygen vacancies. The weight loss is due to the thermal decomposition or dehydration of Co_2O_4 to Co_3O_4 particles.

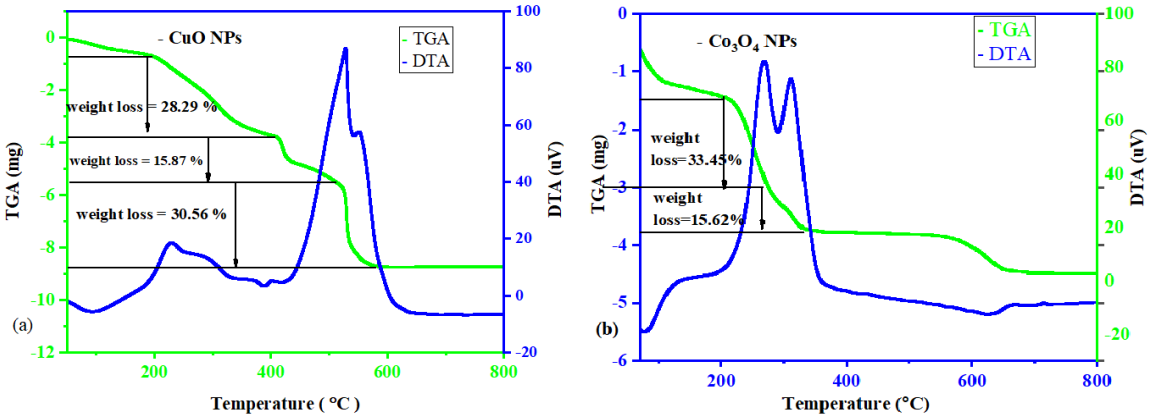

Figure 18: TGA and DTA results of a) CuO NPs and b) Co_3O_4 NPs

4.7 Antibacterial activity of Synthesized Nanoparticles

In this section, the antibacterial activities of the synthesized NPs were discussed. The antibacterial activity of synthesized CuO NPs, Co_3O_4 NPs, and CuO-Co_3O_4 composite NPs with *Moringa stenopetala* leaf extract was investigated using the agar disk diffusion method. Figures 19- 21 show, the antibacterial activity of the synthesized CuO NPs, Co_3O_4 NPs, and CuO-Co_3O_4 composite NPs against the bacterial strains gram-negative *Escherichia coli* (ATCC25922*)* and *Pseudomonas aeruginosa* (ATCC27853), and gram-positive *Staphylococcus aureus*(ATCC25923) and *Streptococcus pyogenes*(ATCC19615).

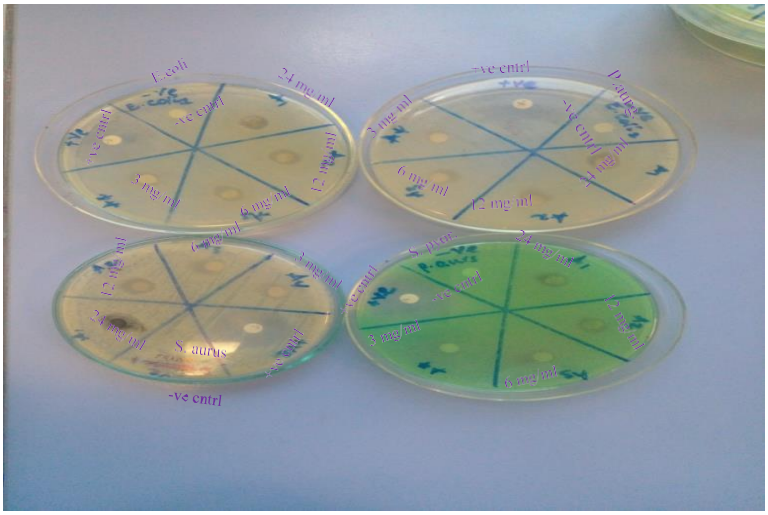

Figure 19: Antibacterial activities of CuO NPs against gram-negative Escherichia coli and Pseudomonas aeruginosa and gram-positive Staphylococcus aureus and Streptococcus pyogenes.

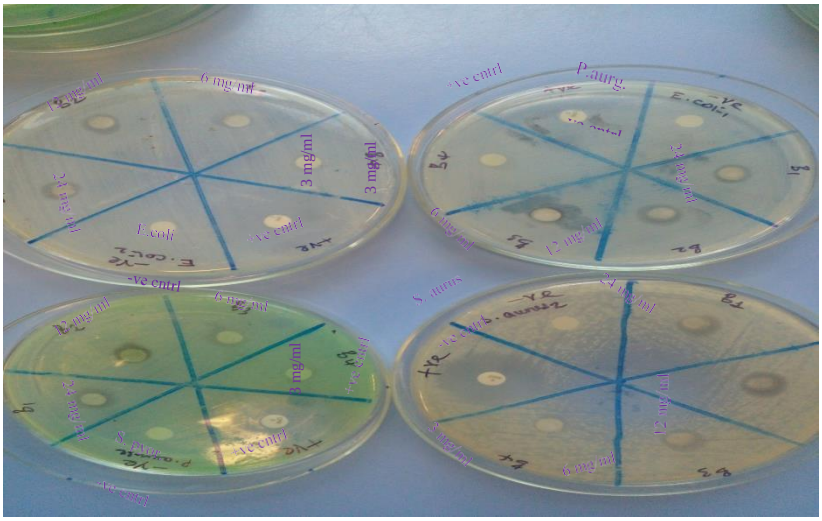

Figure 20: Antibacterial activities of Co_3O_4 NPs against gram-negative Escherichia coli and Pseudomonas aeruginosa and gram-positive Staphylococcus aureus and Streptococcus pyogenes.

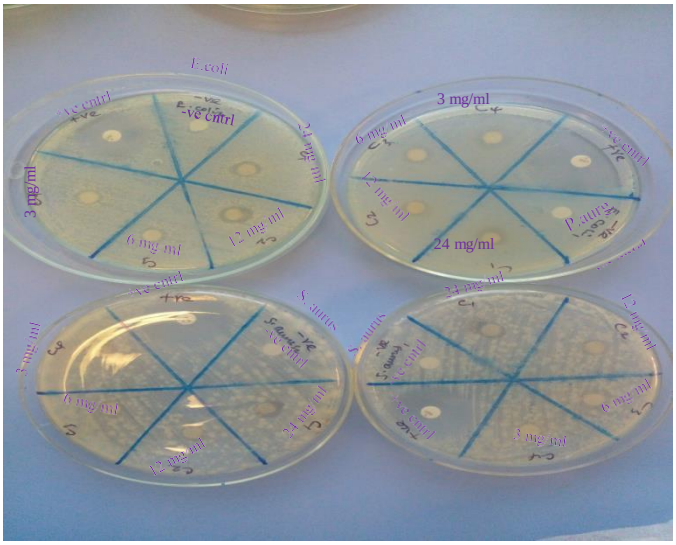

Figure 21: Antibacterial activities of CuO-Co_3O_4 composite NPs against gram-negative Escherichia coli and Pseudomonas aeruginosa and gram-positive Staphylococcus aureus and Streptococcus pyogenes.

The antibacterial activity of the synthesized CuO NPs, Co_3O_4 NPs, and CuO-Co_3O_4 composite NPs against the bacterial strains gram-negative *Escherichia coli* and *Pseudomonas aeruginosa* and gram-positive *Staphylococcus aureus* and *Streptococcus pyogenes* were tabulated and discussed in Tables (5, 6) and 7) respectively.

Table 5: Zones of inhibition of CuO NPs and Gentamicin (+ve control) with different concentrations against different bacterial strains.

Sample	Concentration(mg/mL)	Zone of Inhibition (mm)			
		Gram-negative species		Gram-positive species	
		Escherichia-coli	*Pseudomonas aeruginosa*	*Staphylococcus aureus*	*Streptococcus pyogenes*
CuO NPs	24	11.06 ± 0.25	12.2 ± 0.7	13.6 ± 0.5	11.3 ± 0.5
	12	10.1 ± 0.1	11.66 ± 0.5	12.66 ± 0.5	10.5 ± 0.25
	6	8.66 ± 0.5	11 ± 0.5	11.8 ± 0.3	8.83 ± 0.45
	3	7.66 ± 0.5	9.33 ± 0.5	11.13 ± 0.3	7.5 ± 0.75
Gentamicin (+ve) control		16 ± 0.25	16 ± 0.3	16 ± 0.1	16 ± 0.1
DMSO (-ve) control		6	6	6	6

Table 6: Zones of inhibition of Co_3O_4 NPs NPs and Gentamicin (+ve control) with different concentrations against different bacterial strains.

Sample	Concentration(mg/mL)	Zone of Inhibition (mm)			
		Gram-negative species		Gram-positive species	
		Escherichia-coli	*Pseudomonas aeruginosa*	*Staphylococcus aureus*	*Streptococcus pyogenes*
Co_3O_4 NPs	24	11.66 ± 0.25	13.66 ± 0.5	11 ± 0	11.34 ± 0.65
	12	10.1 ± 0.1	12.4 ± 0.1	10.1 ± 0.35	10.66 ± 0.5
	6	8.66 ± 0.5	11.83 ± 0.25	8.5 ± 0.25	8.8 ± 0.65
	3	7.7 ± 0.55	10.66 ± 0.5	7.66 ± 0.5	7.83 ± 0.25
Gentamicin (+ve) control		16 ± 0.1	16 ± 0.5	16 ± 0.3	16 ± 0.1
DMSO (-ve) control		6	6	6	6

Table 7: Zones of inhibition of CuO-Co_3O_4 Composite NPs and Gentamicin (+ve control) with different concentrations against different bacterial strains

Sample	Concentration(mg/mL)	Zone of Inhibition (mm)			
		Gram-negative species		Gram-positive species	
		Escherichia-coli	*Pseudomonas aeruginosa*	*Staphylococcus aureus*	*Streptococcus pyogenes*
CuO-Co_3O_4 Comosite NPs	24	15	14.66 ± 0.5	13	12.66 ± 0.5
	12	13.73 ± 0.6	13.5 ± 0.75	11.76 ± 0.65	11.7 ± 0.55
	6	12.76 ± 0.65	12.6 ± 0.9	10.8 ± 0.7	10.7 ± 0.6
	3	11.46 ± 0.7	11.23 ± 0.35	9.83 ± 0.75	9.76 ± 0.65
Gentamicin (+ve) control		18 ± 0	18± 0.1	18 ± 0	18 ± 0
DMSO (-ve) control		6	6	6	6

As shown in Figures (19, 20, and 21) supported by Tables (5, 6, and 7), the antibacterial activity of the synthesized CuO NPs, Co_3O_4 NPs, and CuO-Co_3O_4 composite NPs was enhanced with increasing concentration of the nanoparticles. The presence of an inhibition zone indicates that the mechanism of biocidal action of synthesized nanoparticles involves the destruction of the cell membrane of bacterial species and eventually leads to the death of pathogens. Thus, the size of the zone of inhibition varied depending on the type of pathogens, the concentration of synthesized nanoparticles, and the type of nanoparticles.

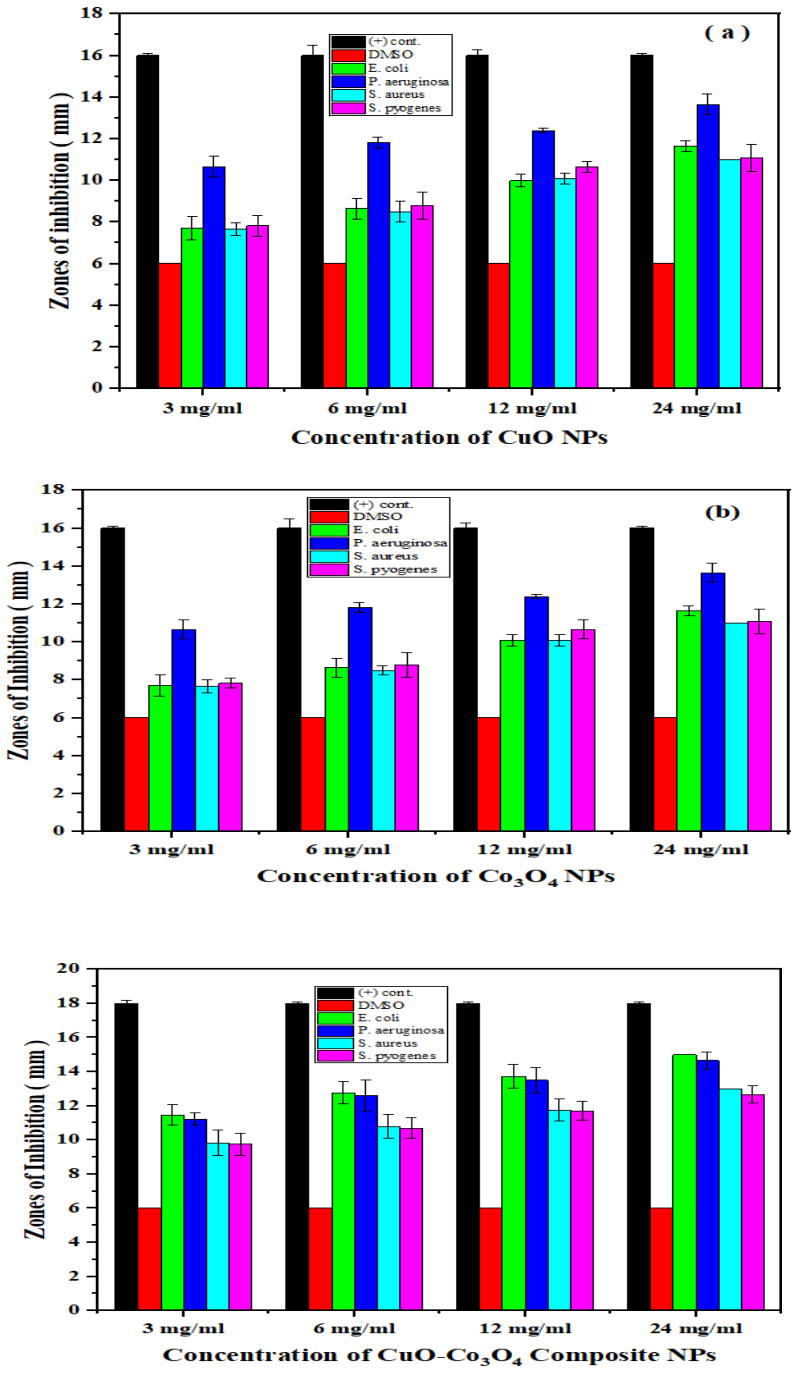

Figure 22: Inhibition Zone of CuO NPs, Co_3O_4 NPs, and CuO-Co_3O_4 composite Nanoparticles against gram-negative Escherichia coli and Pseudomonas aeruginosa and gram-positive Staphylococcus aureus and Streptococcus pyogenes respectively.

Comparing the antibacterial activity of synthesized CuO NPs, Co_3O_4 NPs, and CuO-Co_3O_4 composite NPs against selected bacterial strains *Escherichia coli, Pseudomonas aeruginosa, Staphylococcus aureus,* and *Streptococcus pyogenes*. The CuO-Co_3O_4 composite NPs showed the best inhibitory activities against the selected bacterial species (*Escherichia coli, Pseudomonas aeruginosa,* and *Streptococcus pyogenes*) than the inhibitory activities of CuO NPs and Co_3O_4 NPs. However, CuO NPs showed the best inhibitory effects against bacterial species (*Staphylococcus aureus*) that were not both Co_3O_4 NPs and CuO-Co_3O_4 composite NPs, and Co_3O_4 NPs showed the best inhibitory effects against selected bacterial species (*Escherichia coli, Pseudomonas aeruginosa,* and *Streptococcus pyogenes*), except CuO NPs. and CuO NPs showed the lowest inhibitory activity against selected bacterial species (*Escherichia coli, Pseudomonas aeruginosa,* and *Streptococcus pyogenes*) compared to Co_3O_4 NPs and CuO-Co_3O_4 composite NPs. The result result obtained from research has a strong agreement with previous literature, it can be an indication of the validity and reliability of the research findings. It means that the results are consistent with the existing body of knowledge in the field and support the current understanding of the topic(Peddi et al., 2021)(Hajri et al., 2022).

4.8 Antioxidant activity of synthesized Nanoparticles

The antioxidant activity of DPPH is considered to be a stable source of free radicals and possesses an unpaired electron with a conjugated system. This conjugation of DPPH is responsible for the deep purple color in methanol. When a compound containing an electron-rich substituent and showing a general tendency to donate electrons is mixed with a DPPH solution, DPPH is reduced due to the availability of the odd electron on the nitrogen atom. This disrupts the conjugation of DPPH and converts it into a diamagnetic molecule. This transformation is complemented by the color change of the solution from deep violet to pale yellow. This transformation also leads to a reduction in the intensity of the UV-Vis peak of DPPH at 517 nm. The resulting discoloration is stoichiometric concerning the number of electrons accepted(Das & Saikia, 2022).

The antioxidant activity of the biosynthesized nanoparticles was investigated at different concentrations ranging from 10-40 mg/mL. As the surface reactions between synthesized nanoparticles (CuO NPs, Co_3O_4 NPs, and CuO-Co_3O_4 composite NPs), and the DPPH solution

proceeded, the color of the solution slowly changed from deep violet to pale yellow. A gradual increase in the peak intensity of the synthesized nanoparticle solution at 517 nm with increasing concentration was observed by UV-Vis analysis (Fig. 23).

The color change of the DPPH solution as well as the magnitude of the increase in the UV-visible peak intensity in the presence of CuO NPs, Co_3O_4 NPs, and CuO-Co_3O_4 composite NPs gives the visual monitoring of the antioxidant activity of the synthesized nanoparticles. By determining the UV-visible peak intensity of the control and the considered supernatant solution at different concentrations, the percentage of antioxidant activity of the synthesized nanoparticles when varying the concentration was given in Fig. 23, which shows a gradual increase in antioxidant activity with increasing concentration CuO NPs, Co_3O_4 NPs, and CuO-Co_3O_4 composite NPs. The results of the DPPH inhibition study are shown in Table 8 and the comparative graph is shown in Figure 23.

Table 8: Results obtained in DPPH radical scavenging assay

S. No	Concentration(mg/mL)	% of DPPH Inhibition		
		CuO NPs	Co_3O_4 NPs	CuO-Co_3O_4 Composite NPs
1	10	49.2	66.6	69.2
2	20	53.9	69.2	72.9
3	30	59.6	72.9	77.8
4	40	62.6	75.3	81.9

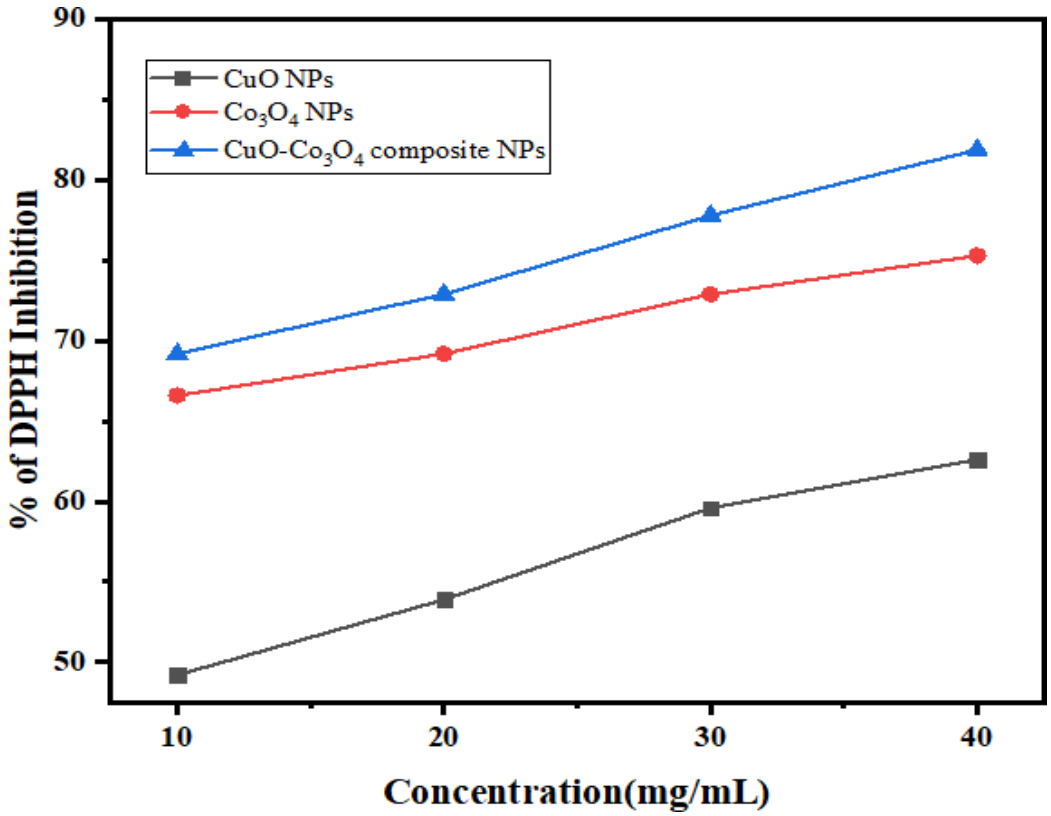

Figure 23: Comparative graph of DPPH assay study results of CuO NPs, Co_3O_4 NPs, and CuO-Co_3O_4 composite NPs at different concentrations.

The DPPH radical test of CuO NPs, Co_3O_4 NPs, and CuO-Co_3O_4 composite NPs compared to each other. The results confirm that the CuO-Co_3O_4 composite NPs have the best and highest DPPH inhibitory activity compared to CuO NPs and Co_3O_4 NPs and that the Co_3O_4 NPs also showed increased radical inhibitory activity than CuO NPs compared to the green synthesized CuO NPs showed the lowest antioxidant activity. At a concentration of 40 (mg/mL), a scavenging capacity of CuO-Co_3O_4 composite NPs of up to 81.9% was achieved. This shows that synthetic CuO-Co_3O_4 composite nanoparticles exhibit the highest antioxidant activity. This result agreed with a previous literature(Peddi et al., 2021)(Hajri et al., 2022).

CHAPTER FIVE

CONCLUSION AND RECOMMENDATION

5.1 Conclusion

In conclusion, the green synthesis of CuO NPs, Co_3O_4 NPs, and CuO-Co_3O_4 composite NPs using *Moringa stenopetala* leaf extract as a reducing agent provides a promising approach for the synthesis of nanoparticles with unique properties. The synthesized nanoparticles were characterized using various techniques, such as UV-Vis spectrophotometer, XRD, SEM, FTIR, and TGA, revealing their distinct properties and potential for various applications. Among the synthesized nanoparticles, the CuO-Co_3O_4 composite NPs showed superior properties and advantages over other synthesized nanoparticles.

The CuO-Co_3O_4 composite NPs exhibit a unique composition that combines the properties of both CuO and Co_3O_4 NPs, providing them with enhanced synergistic effects and increased stability. The results of this study suggest that the CuO-Co_3O_4 composite NPs hold great potential for various applications, given their superior inhibitory and radical inhibitory activity. Additionally, the CuO-Co_3O_4 composite NPs have a high surface area-to-volume ratio, which enables them to interact efficiently with other molecules and biological systems, making them ideal candidates for various biomedical applications.

In addition, the CuO-Co_3O_4 composite NPs synthesized in this study have several advantages over other nanoparticles. One of the main advantages is that they have a high surface area-to-volume ratio, which enables them to interact efficiently with other molecules and biological systems, making them ideal candidates for various biomedical applications. Furthermore, the CuO-Co_3O_4 composite NPs have a unique composition that combines the properties of both CuO and Co_3O_4 NPs, providing them with enhanced synergistic effects and increased stability.

Another advantage of the CuO-Co_3O_4 composite NPs is their excellent biocompatibility, which makes them suitable for use in various in vivo and in vitro applications. Additionally, the green synthesis method used in this study is an eco-friendly and sustainable approach that produces

nanoparticles with minimal environmental impact, making it an attractive alternative to conventional synthesis methods. Overall, the results of this study demonstrate the potential of CuO-Co_3O_4 composite NPs synthesized via green synthesis as a promising candidate for various biomedical and environmental applications, given their unique properties and advantages over other nanoparticles.

5.2 Recommendation

Based on the key findings and conclusions of the study, the following points were recommended: The synthesis of metal oxide nanoparticles and composite NPs with environmentally friendly methods is one of the emerging research areas with great prospects. Therefore, advanced studies should be carried out on the synthesis of CuO-Co_3O_4 composite NPs and their applications, for example, in the field of optoelectronic devices, electrochemical, photocatalytic, and other biomedical applications.

This study only focused on examining the effect of the synthesized CuO NPs, Co_3O_4 NPs, and CuO-Co_3O_4 composite NPs against four different bacterial strains. Therefore, further research on an expanded spectrum of human pathogens is required for understanding their full extent. Also, I recommend that the synthesized nanoparticles be further characterized by different tools like EDX, TEM, HRTEM, and DLS analysis.

Research Fund Acknowledgment

This work is financially supported by Adama Science and Technology University and the Ministry of Innovation and Technology of Ethiopia under the grant number ASTU/SM-R/684/23, Adama, Ethiopia.

6. REFERENCES

Abebe, B., Murthy, H. C. A., Zereffa, E. A., & Adimasu, Y. (2021). Synthesis and characterization of ZnO/PVA nanocomposites for antibacterial and electrochemical applications. *Inorganic and Nano-Metal Chemistry*, *51*(8), 1127–1138. https://doi.org/10.1080/24701556.2020.1814338

Ahmad, A., Mukherjee, P., Senapati, S., Mandal, D., Khan, M. I., Kumar, R., & Sastry, M. (2003). Extracellular biosynthesis of silver nanoparticles using the fungus Fusarium oxysporum. *Colloids and Surfaces B: Biointerfaces*, *28*(4), 313–318. https://doi.org/10.1016/S0927-7765(02)00174-1

Akilandaeaswari, B., & Muthu, K. (2021). One-pot green synthesis of Au-Ag bimetallic nanoparticles from Lawsonia inermis seed extract and its catalytic reduction of environmental polluted methyl orange and 4-nitrophenol. *Journal of the Taiwan Institute of Chemical Engineers*, *127*, 292–301. https://doi.org/10.1016/j.jtice.2021.07.019

Akinsiku, A. A., Dare, E. O., Ajani, O. O., Ayo-Ajayi, J., Ademosun, O. T., & Ajayi, S. O. (2018). Room temperature Phytosynthesis of Ag/Co bimetallic nanoparticles using aqueous leaf extract of Canna indica. *IOP Conference Series: Earth and Environmental Science*, *173*(1). https://doi.org/10.1088/1755-1315/173/1/012019

Akintelu, S. A., Folorunso, A. S., Folorunso, F. A., & Oyebamiji, A. K. (2020). Green synthesis of copper oxide nanoparticles for biomedical application and environmental remediation. *Heliyon*, *6*(7), e04508. https://doi.org/10.1016/j.heliyon.2020.e04508

Al-Haddad, J., Alzaabi, F., Pal, P., Rambabu, K., & Banat, F. (2020). Green synthesis of bimetallic copper–silver nanoparticles and their application in catalytic and antibacterial activities. *Clean Technologies and Environmental Policy*, *22*(1), 269–277. https://doi.org/10.1007/s10098-019-01765-2

Amal, N., & Mohamad, N. (2013). *A Short Review on the Synthesis of Bimetallic Nanoparticles using Plant Extract*. 334–339.

Andualem, W. W., Sabir, F. K., Mohammed, E. T., Belay, H. H., & Gonfa, B. A. (2020).

Synthesis of copper oxide nanoparticles using plant leaf extract of catha edulis and its antibacterial activity. *Journal of Nanotechnology*, *2020*. https://doi.org/10.1155/2020/2932434

Aragaw, S. G., Sabir, F. K., Andoshe, D. M., & Zelekew, O. A. (2020). Green synthesis of p-Co3O4/n-ZnO composite catalyst with Eichhornia crassipes plant extract mediated for methylene blue degradation under visible light irradiation. *Materials Research Express*, *7*(9). https://doi.org/10.1088/2053-1591/abb90e

Awad, A. M., Kumar, P., Ismail-Fitry, M. R., Jusoh, S., Ab Aziz, M. F., & Sazili, A. Q. (2021). Green extraction of bioactive compounds from plant biomass and their application in meat as natural antioxidant. *Antioxidants*, *10*(9), 1–39. https://doi.org/10.3390/antiox10091465

Azizian-Shermeh, O., Valizadeh, M., Taherizadeh, M., & Beigomi, M. (2020). Phytochemical investigation and phytosynthesis of eco-friendly stable bioactive gold and silver nanoparticles using petal extract of saffron (Crocus sativus L.) and study of their antimicrobial activities. *Applied Nanoscience (Switzerland)*, *10*(8), 2907–2920. https://doi.org/10.1007/s13204-019-01059-5

Baptista, P. V., McCusker, M. P., Carvalho, A., Ferreira, D. A., Mohan, N. M., Martins, M., & Fernandes, A. R. (2018). Nano-strategies to fight multidrug resistant bacteria-"A Battle of the Titans". *Frontiers in Microbiology*, *9*(JUL), 1–26. https://doi.org/10.3389/fmicb.2018.01441

Behzad, F., Naghib, S. M., kouhbanani, M. A. J., Tabatabaei, S. N., Zare, Y., & Rhee, K. Y. (2021). An overview of the plant-mediated green synthesis of noble metal nanoparticles for antibacterial applications. *Journal of Industrial and Engineering Chemistry*, *94*, 92–104. https://doi.org/10.1016/j.jiec.2020.12.005

Bekele, E. T., Murthy, H. C. A., Muniswamy, D., Lemenh, Y. A., Shume, M. S., Tadesse Ayanie, G., Kumar, A. P., Ravikumar, C. R., Balachandran, R., & Roy, A. (2022). Solanum tuberosum Leaf Extract Templated Synthesis of Co3O4Nanoparticles for Electrochemical Sensor and Antibacterial Applications. *Bioinorganic Chemistry and Applications*, *2022*(16 mm). https://doi.org/10.1155/2022/8440756

Bekru, A. G., Tufa, L. T., Zelekew, O. A., Goddati, M., Lee, J., & Sabir, F. K. (2022). Green Synthesis of a CuO-ZnO Nanocomposite for Efficient Photodegradation of Methylene Blue and Reduction of 4-Nitrophenol. *ACS Omega*, *7*(35), 30908–30919. https://doi.org/10.1021/acsomega.2c02687

Benhammada, A., & Trache, D. (2022). Green synthesis of CuO nanoparticles using Malva sylvestris leaf extract with different copper precursors and their effect on nitrocellulose thermal behavior. *Journal of Thermal Analysis and Calorimetry*, *147*(2), 1355–1370. https://doi.org/10.1007/s10973-020-10469-5

Bhargava, R., Khan, S., Ahmad, N., Mohsin, M., & Ansari, N. (2018). *Investigation of Structural , Optical and Electrical Properties of Co 3 O 4 Nanoparticles*. *030034*, 1–5. https://doi.org/10.1063/1.5032369

Bibi, I., Nazar, N., Iqbal, M., Kamal, S., Nawaz, H., Nouren, S., Safa, Y., Jilani, K., Sultan, M., Ata, S., Rehman, F., & Abbas, M. (2017). Green and eco-friendly synthesis of cobalt-oxide nanoparticle: Characterization and photo-catalytic activity. *Advanced Powder Technology*, *28*(9), 2035–2043. https://doi.org/10.1016/j.apt.2017.05.008

Burlacu, E., Nisca, A., & Tanase, C. (2020). A comprehensive review of phytochemistry and biological activities of Quercus species. *Forests*, *11*(9), 1–24. https://doi.org/10.3390/F11090904

Chakraborty, N., Banerjee, J., Chakraborty, P., Banerjee, A., Chanda, S., Ray, K., Acharya, K., & Sarkar, J. (2022). Green synthesis of copper/copper oxide nanoparticles and their applications: a review. *Green Chemistry Letters and Reviews*, *15*(1), 185–213. https://doi.org/10.1080/17518253.2022.2025916

Chatterjee, K., Sarkar, S., Jagajjanani Rao, K., & Paria, S. (2014). Core/shell nanoparticles in biomedical applications. *Advances in Colloid and Interface Science*, *209*, 8–39. https://doi.org/10.1016/j.cis.2013.12.008

Dalvand, A., Gholibegloo, E., Ganjali, M. R., Golchinpoor, N., Khazaei, M., Kamani, H., Hosseini, S. S., & Mahvi, A. H. (2016). Comparison of Moringa stenopetala seed extract as

a clean coagulant with Alum and Moringa stenopetala-Alum hybrid coagulant to remove direct dye from Textile Wastewater. *Environmental Science and Pollution Research*, *23*(16), 16396–16405. https://doi.org/10.1007/s11356-016-6708-z

Das, D., Nath, B. C., Phukon, P., & Dolui, S. K. (2013). Synthesis and evaluation of antioxidant and antibacterial behavior of CuO nanoparticles. *Colloids and Surfaces B: Biointerfaces*, *101*, 430–433. https://doi.org/10.1016/j.colsurfb.2012.07.002

Das, D., & Saikia, B. J. (2022). Synthesis, Characterization and Biological Applications of Cobalt Oxide (Co3o4) Nanoparticles. *SSRN Electronic Journal*, 100137. https://doi.org/10.2139/ssrn.4172613

Diallo, A., Beye, A. C., Doyle, T. B., Park, E., Maaza, M., Beye, A. C., Doyle, T. B., Park, E., & Green, M. M. (2015). *Green Chemistry Letters and Reviews Green synthesis of Co 3 O 4 nanoparticles via Aspalathus linearis : Physical properties*. *8253*. https://doi.org/10.1080/17518253.2015.1082646

Din, M. I., & Rehan, R. (2017). Synthesis , Characterization , and Applications of Copper Nanoparticles. *Analytical Letters*, *50*(1), 50–62. https://doi.org/10.1080/00032719.2016.1172081

Dobrucka, R. (2018). Antioxidant and Catalytic Activity of Biosynthesized CuO Nanoparticles Using Extract of Galeopsidis herba. *Journal of Inorganic and Organometallic Polymers and Materials*, *28*(3), 812–819. https://doi.org/10.1007/s10904-017-0750-2

Domènech, B., Ziegler, K., Vigués, N., Olszewski, W., Marini, C., Mas, J., Muñoz, M., Muraviev, D. N., & Macanás, J. (2016). Polyurethane foams doped with stable silver nanoparticles as bactericidal and catalytic materials for the effective treatment of water. In *New Journal of Chemistry* (Vol. 40, Issue 4, pp. 3716–3725). https://doi.org/10.1039/c5nj03202d

Dsouza, A., Shilpa, M. P., Gurumurthy, S. C., Nagaraja, B. S., Mundinamani, S., Ramam, K., Gedda, M., & Murari, M. S. (2021). CuAg and AuAg bimetallic nanoparticles for catalytic and heat transfer applications. *Clean Technologies and Environmental Policy*, *23*(7), 2145–

2155. https://doi.org/10.1007/s10098-021-02120-0

Ebenezar Udofia, N., Jared Misonge, O., Mworia, M., William, N., & Gervason Apiri, M. (2020). Chemical Composition of Moringa oleifera Lam. and Moringa stenopetala Bac. Leaves from Kenya. *International Journal of Plant Research*, *2020*(1), 1–10. https://doi.org/10.5923/j.plant.20201001.01

Eltarahony, M., Zaki, S., Elkady, M., & Abd-El-Haleem, D. (2018). Biosynthesis, Characterization of Some Combined Nanoparticles, and Its Biocide Potency against a Broad Spectrum of Pathogens. *Journal of Nanomaterials*, *2018*. https://doi.org/10.1155/2018/5263814

Engineering, C., & Kamal, I. (2017). *Chemistry & Nanotechnology PhD , Polymer Technology*. *August*. https://doi.org/10.13140/RG.2.2.19999.25769

Fu, T., Fang, J., Wang, C., & Zhao, J. (2016). Hollow porous nanoparticles with Pt skin on a Ag-Pt alloy structure as a highly active electrocatalyst for the oxygen reduction reaction. *Journal of Materials Chemistry A*, *4*(22), 8803–8811. https://doi.org/10.1039/c6ta02202b

Gallon, J. R., Kittakoop, P., & Brown, E. G. (1994). Biosynthesis of anatoxin-a byAnabaena flos-aquae: Examination of primary enzymic steps. *Phytochemistry*, *35*(5), 1195–1203. https://doi.org/10.1016/S0031-9422(00)94821-0

Ganaie, S. U., Abbasi, T., & Abbasi, S. A. (2016). Rapid and green synthesis of bimetallic Au–Ag nanoparticles using an otherwise worthless weed Antigonon leptopus. *Journal of Experimental Nanoscience*, *11*(6), 395–417. https://doi.org/10.1080/17458080.2015.1070311

Ghosh, S., Nitnavare, R., Dewle, A., Tomar, G. B., Chippalkatti, R., More, P., Kitture, R., Kale, S., Bellare, J., & Chopade, B. A. (2015). Novel platinum–palladium bimetallic nanoparticles synthesized by Dioscorea bulbifera: Anticancer and antioxidant activities. *International Journal of Nanomedicine*, *10*, 7477–7490. https://doi.org/10.2147/IJN.S91579

Gopinath, K., Kumaraguru, S., Bhakyaraj, K., Mohan, S., Venkatesh, K. S., Esakkirajan, M., Kaleeswarran, P., Alharbi, N. S., Kadaikunnan, S., Govindarajan, M., Benelli, G., &

Arumugam, A. (2016). Green synthesis of silver, gold and silver/gold bimetallic nanoparticles using the Gloriosa superba leaf extract and their antibacterial and antibiofilm activities. In *Microbial Pathogenesis* (Vol. 101). https://doi.org/10.1016/j.micpath.2016.10.011

Govindasamy, R., Raja, V., Singh, S., Govindarasu, M., Sabura, S., Rekha, K., Rajeswari, V. D., Alharthi, S. S., Vaiyapuri, M., Sudarmani, R., Jesurani, S., Venkidasamy, B., & Thiruvengadam, M. (2022a). Green Synthesis and Characterization of Cobalt Oxide Nanoparticles Using Psidium guajava Leaves Extracts and Their Photocatalytic and Biological Activities. *Molecules*, *27*(17), 1–16. https://doi.org/10.3390/molecules27175646

Govindasamy, R., Raja, V., Singh, S., Govindarasu, M., Sabura, S., Rekha, K., Rajeswari, V. D., Alharthi, S. S., Vaiyapuri, M., Sudarmani, R., Jesurani, S., Venkidasamy, B., & Thiruvengadam, M. (2022b). Green Synthesis and Characterization of Cobalt Oxide Nanoparticles Using Psidium guajava Leaves Extracts and Their Photocatalytic and Biological Activities. *Molecules*, *27*(17). https://doi.org/10.3390/molecules27175646

Guisbiers, G., Mendoza-Cruz, R., Bazán-Díaz, L., Velázquez-Salazar, J. J., Mendoza-Perez, R., Robledo-Torres, J. A., Rodriguez-Lopez, J. L., Montejano-Carrizales, J. M., Whetten, R. L., & José-Yacamán, M. (2016). Electrum, the gold-silver alloy, from the bulk scale to the nanoscale: Synthesis, properties, and segregation rules. *ACS Nano*, *10*(1), 188–198. https://doi.org/10.1021/acsnano.5b05755

Habtemariam, S., & Varghese, G. K. (2015). Extractability of rutin in herbal tea preparations of moringa stenopetala leaves. *Beverages*, *1*(3), 169–182. https://doi.org/10.3390/beverages1030169

Hajri, A. K., Albalawi, M. A., Alsharif, I., & Jamoussi, B. (2022). Marine Algae Extract (Grateloupia Sparsa) for the Green Synthesis of Co3O4NPs: Antioxidant, Antibacterial, Anticancer, and Hemolytic Activities. *Bioinorganic Chemistry and Applications*, *2022*, 1–11. https://doi.org/10.1155/2022/3977935

Iravani, S., & Varma, R. S. (2020). Sustainable synthesis of cobalt and cobalt oxide nanoparticles and their catalytic and biomedical applications. *Green Chemistry*, *22*(9),

2643–2661. https://doi.org/10.1039/d0gc00885k

Kassim, M., Achoui, M., Mustafa, M. R., Mohd, M. A., & Yusoff, K. M. (2010). Ellagic acid, phenolic acids, and flavonoids in Malaysian honey extracts demonstrate in vitro anti-inflammatory activity. *Nutrition Research*, *30*(9), 650–659. https://doi.org/10.1016/j.nutres.2010.08.008

Khodamorady, M., Sohrabnezhad, S., & Bahrami, K. (2020). Efficient one-pot synthetic methods for the preparation of 3,4-dihydropyrimidinones and 1,4-dihydropyridine derivatives using BNPs@SiO2(CH2)3NHSO3H as a ligand and metal free acidic heterogeneous nano-catalyst. *Polyhedron*, *178*(3), 114340. https://doi.org/10.1016/j.poly.2019.114340

Krishna, B. A., Kumar, P. N., & Prema, P. (2020). Green synthesis of copper oxide nanoparticles using Cinnamomum malabatrum leaf extract and its antibacterial activity. *Indian Journal of Chemical Technology*, *27*(6), 525–530. https://doi.org/10.56042/ijct.v27i6.34504

Lebovitz, H. E. (1997). Alpha-glucosidase inhibitors. *Endocrinology and Metabolism Clinics of North America*, *26*(3), 539–551. https://doi.org/10.1016/S0889-8529(05)70266-8

Love, A. J., Makarov, V. V., Sinitsyna, O. V., Shaw, J., Yaminsky, I. V., Kalinina, N. O., & Taliansky, M. E. (2015). A genetically modified tobacco mosaic virus that can produce gold nanoparticles from a metal salt precursor. *Frontiers in Plant Science*, *6*(NOVEMBER), 1–10. https://doi.org/10.3389/fpls.2015.00984

Loza, K., Heggen, M., & Epple, M. (2020). Synthesis, Structure, Properties, and Applications of Bimetallic Nanoparticles of Noble Metals. *Advanced Functional Materials*, *30*(21). https://doi.org/10.1002/adfm.201909260

Martinello, M., & Mutinelli, F. (2021). Antioxidant activity in bee products: A review. *Antioxidants*, *10*(1), 1–42. https://doi.org/10.3390/antiox10010071

Mauricio, M. D., Guerra-Ojeda, S., Marchio, P., Valles, S. L., Aldasoro, M., Escribano-Lopez, I., Herance, J. R., Rocha, M., Vila, J. M., & Victor, V. M. (2018). Nanoparticles in medicine: A focus on vascular oxidative stress. *Oxidative Medicine and Cellular Longevity*, *2018*. https://doi.org/10.1155/2018/6231482

McClements, D. J., & Öztürk, B. (2022). Utilization of Nanotechnology to Improve the Application and Bioavailability of Phytochemicals Derived from Waste Streams. *Journal of Agricultural and Food Chemistry*, *70*(23), 6884–6900. https://doi.org/10.1021/acs.jafc.1c03020

Md Ishak, N. A. I., Kamarudin, S. K., & Timmiati, S. N. (2019). Green synthesis of metal and metal oxide nanoparticles via plant extracts: an overview. *Materials Research Express*, *6*(11). https://doi.org/10.1088/2053-1591/ab4458

Meghdadi, S., Amirnasr, M., Zhiani, M., Jallili, F., Jari, M., & Kiani, M. (2017). Facile Synthesis of Cobalt Oxide Nanoparticles by Thermal Decomposition of Cobalt(II) Carboxamide Complexes: Application as Oxygen Evolution Reaction Electrocatalyst in Alkaline Water Electrolysis. *Electrocatalysis*, *8*(2), 122–131. https://doi.org/10.1007/s12678-016-0345-7

Mittal, A. K., Kumar, S., & Banerjee, U. C. (2014). Quercetin and gallic acid mediated synthesis of bimetallic (silver and selenium) nanoparticles and their antitumor and antimicrobial potential. *Journal of Colloid and Interface Science*, *431*, 194–199. https://doi.org/10.1016/j.jcis.2014.06.030

Mounika, K., Pragathi, A., & Gyanakumari, C. (2010). Synthesis¸ Characterization and Biological Activity of a Schiff Base Derived from 3-Ethoxy Salicylaldehyde and 2-Amino Benzoic acid and its Transition Metal Complexes. *Journal of Scientific Research*. https://doi.org/10.3329/jsr.v2i3.4899

Mungondori, H. H., Ramujana, S., Katwire, D. M., & Taziwa, R. T. (2018). Synthesis of a novel visible light responsive γ-Fe 2 O 3 /SiO 2 / C-TiO 2 magnetic nanocomposite for water treatment. *Water Science and Technology*, *78*(12), 2500–2510. https://doi.org/10.2166/wst.2019.004

Mutukwa, D., & Taziwa, R. (2022). *A Review of the Green Synthesis of ZnO Nanoparticles Utilising Southern African Indigenous Medicinal Plants*.

Mutukwa, D., Taziwa, R., & Khotseng, L. E. (2022). A Review of the Green Synthesis of ZnO Nanoparticles Utilising Southern African Indigenous Medicinal Plants. *Nanomaterials*,

12(19). https://doi.org/10.3390/nano12193456

Naika, H. R., Lingaraju, K., Manjunath, K., Kumar, D., Nagaraju, G., & Nagabhushana, H. (2018). Green synthesis of CuO nanoparticles using Gloriosa superba L . extract and their antibacterial activity Green synthesis of CuO nanoparticles using Gloriosa superba L . extract and their antibacterial activity. *Integrative Medicine Research*, *9*(1), 7–12. https://doi.org/10.1016/j.jtusci.2014.04.006

Narayana, K. R., Reddy, M. S., Chaluvadi, M. R., & Krishna, D. R. (2001). Bioflavonoids classification, pharmacological, biochemical effects and therapeutic potential. *Indian Journal of Pharmacology*, *33*(1), 2–16.

Nasrabadi, H. T., Abbasi, E., Davaran, S., Kouhi, M., & Akbarzadeh, A. (2016). Bimetallic nanoparticles: Preparation, properties, and biomedical applications. *Artificial Cells, Nanomedicine and Biotechnology*, *44*(1), 376–380. https://doi.org/10.3109/21691401.2014.953632

Panchal, P., & Parvez, N. (2019). Phytochemical analysis of medicinal herb (ocimum sanctum). *International Journal of Nanomaterials, Nanotechnology and Nanomedicine*, *5*(2), 008–011. https://doi.org/10.17352/2455-3492.000029

Pantidos, N. (2014). Biological Synthesis of Metallic Nanoparticles by Bacteria, Fungi and Plants. *Journal of Nanomedicine & Nanotechnology*, *05*(05). https://doi.org/10.4172/2157-7439.1000233

Patil, S., Venckatesh, R., & Seenivasan, R. (2015). Green synthesis of silver nanoparticle from leaf extract of aegle marmelos and evaluation of its antibacterial activity. *International Journal of Pharmacy and Pharmaceutical Sciences*, *7*(6), 169–173.

Peddi, P., Ptsrk, P. R., Rani, N. U., & Tulasi, S. L. (2021). Green synthesis, characterization, antioxidant, antibacterial, and photocatalytic activity of Suaeda maritima (L.) Dumort aqueous extract-mediated copper oxide nanoparticles. *Journal of Genetic Engineering and Biotechnology*, *19*(1). https://doi.org/10.1186/s43141-021-00229-9

Prakash, M., Kavitha, H. P., Abinaya, S., Vennila, J. P., & Lohita, D. (2022). Green synthesis of

bismuth based nanoparticles and its applications - A review. *Sustainable Chemistry and Pharmacy*, *25*(February). https://doi.org/10.1016/j.scp.2021.100547

Raja, H. A., Miller, A. N., Pearce, C. J., & Oberlies, N. H. (2017). Fungal Identification Using Molecular Tools: A Primer for the Natural Products Research Community. *Journal of Natural Products*, *80*(3), 756–770. https://doi.org/10.1021/acs.jnatprod.6b01085

Ramezani, N., Ehsanfar, Z., Shamsa, F., Amin, G., Shahverdi, H. R., Monsef Esfahani, H. R., Shamsaie, A., Bazaz, R. D., & Shahverdi, A. R. (2008). Screening of medicinal plant methanol extracts for the synthesis of gold nanoparticles by their reducing potential. *Zeitschrift Fur Naturforschung - Section B Journal of Chemical Sciences*, *63*(7), 903–908. https://doi.org/10.1515/znb-2008-0715

Rastogi, A., Tripathi, D. K., Yadav, S., Chauhan, D. K., Živčák, M., Ghorbanpour, M., El-Sheery, N. I., & Brestic, M. (2019). Application of silicon nanoparticles in agriculture. *3 Biotech*, *9*(3), 1–11. https://doi.org/10.1007/s13205-019-1626-7

Ravikumar, K. V. G., Sudakaran, S. V., Ravichandran, K., Pulimi, M., Natarajan, C., & Mukherjee, A. (2019). Green synthesis of NiFe nano particles using Punica granatum peel extract for tetracycline removal. *Journal of Cleaner Production*, *210*, 767–776. https://doi.org/10.1016/j.jclepro.2018.11.108

Riaz, T., Nayyar, S., Shahzadi, T., Zaib, M., Shahid, S., Mansoor, S., Javed, M., Iqbal, S., Al-anazy, M. M., Elkaeed, E. B., & Pashameah, R. A. (2022). *The Biogenic Synthesis of Cobalt Monometallic and Cobalt – Zinc Bimetallic Nanoparticles Using Cymbopogan citratus L . Leaf Extract and Assessment of Their Activities as Efficient Dye Removal and Antioxidant Agents*.

Roopan, S. M., & Surendra, T. V. (2014). *Biosynthetic trends and future aspects of bimetallic nanoparticles and its medicinal applications*. 5289–5300. https://doi.org/10.1007/s00253-014-5736-1

Saranyaadevi, K., Subha, V., Ernest Ravindran, R. S., & Renganathan, S. (2014). Green synthesis and characterization of silver nanoparticle using leaf extract of Capparis

zeylanica. *Asian Journal of Pharmaceutical and Clinical Research*, *7*(SUPPL. 2), 44–48.

Sayadi, M. H., Ghollasimood, S., Ahmadpour, N., & Homaeigohar, S. (2022). Biosynthesis of the ZnO/SnO2 nanoparticles and characterization of their photocatalytic potential for removal of organic water pollutants. *Journal of Photochemistry and Photobiology A: Chemistry*, *425*. https://doi.org/10.1016/j.jphotochem.2021.113662

Shafey, A. M. El. (2020). Green synthesis of metal and metal oxide nanoparticles from plant leaf extracts and their applications: A review. *Green Processing and Synthesis*, *9*(1), 304–339. https://doi.org/10.1515/gps-2020-0031

Sharif Mughal, S., & Mona Hassan, S. (2022). To cite this article: Shahzad Sharif Mughal, Syeda Mona Hassan. Comparative Study of AgO Nanoparticles Synthesize Via Biological, Chemical and Physical Methods: A Review. *American Journal of Materials Synthesis and Processing*, *7*(2), 15–28. https://doi.org/10.11648/j.ajmsp.20220702.11

Sharma, R. A., Chowdhury, M. A., & Sahu, A. (2022). A Review on Biofabrication of Zinc Nanoparticles, Its Mechanism and Recent Applications. *International Journal of Health Sciences and Research*, *12*(11), 101–120. https://doi.org/10.52403/ijhsr.20221115

Shehu, Z., Lamayi Danbature, W., Magaji, B., Mustapha Adam, M., Aminu Bunu, M., John Mai, A., & Mela, Y. (2020). Green Synthesis and Nanotoxicity Assay of Copper-Cobalt Bimetallic Nanoparticles as a Novel Nanolarvicide for Mosquito Larvae Management. *The International Journal of Biotechnology*, *9*(2), 99–104. https://doi.org/10.18488/journal.57.2020.92.99.104

Shelke, H. D., Machale, A. R., Survase, A. A., Pathan, H. M., Lokhande, C. D., Lokhande, A. C., Shaikh, S. F., Rana, A. U. H. S., & Palaniswami, M. (2022). Multifunctional Cu2SnS3 Nanoparticles with Enhanced Photocatalytic Dye Degradation and Antibacterial Activity. *Materials*, *15*(9). https://doi.org/10.3390/ma15093126

Shumi, L. D. (2019). *Addis Ababa Science and Technology University Studies on Extraction of Moringa Stenopetala Seed Oil : Process Optimization and Investigation of It ' S Potential As Cooking Oil*. *June*.

Singh, A. K. (2022). A review on plant extract-based route for synthesis of cobalt nanoparticles: Photocatalytic, electrochemical sensing and antibacterial applications. *Current Research in Green and Sustainable Chemistry*, *5*(January), 100270. https://doi.org/10.1016/j.crgsc.2022.100270

Subbiah, K. S., & Beedu, S. R. (2018). Biogenic synthesis of biopolymer-based ag–Au bimetallic nanoparticle constructs and their anti-proliferative assessment. *IET Nanobiotechnology*, *12*(8), 1047–1055. https://doi.org/10.1049/iet-nbt.2018.5135

Sun, Y., & Xia, Y. (2003). Shape-Controlled Synthesis of Gold and Silver Nanoparticles. *ChemInform*, *34*(10), 2176–2180. https://doi.org/10.1002/chin.200310226

Thangaswamy, S. J. K., Mir, M. A., & Muthu, A. (2021). Green synthesis of mono and bimetallic alloy nanoparticles of gold and silver using aqueous extract of Chlorella acidophile for potential applications in sensors. *Preparative Biochemistry and Biotechnology*, *51*(10), 1026–1035. https://doi.org/10.1080/10826068.2021.1894441

Usman, A. I., Aziz, A. A., & Noqta, O. A. (2019). Application of green synthesis of gold nanoparticles: A review. *Jurnal Teknologi*, *81*(1), 171–182. https://doi.org/10.11113/jt.v81.11409

Valodkar, M., Modi, S., Pal, A., & Thakore, S. (2011). Synthesis and anti-bacterial activity of Cu, Ag and Cu-Ag alloy nanoparticles: A green approach. *Materials Research Bulletin*, *46*(3), 384–389. https://doi.org/10.1016/j.materresbull.2010.12.001

Varughese, A., Kaur, R., & Singh, P. (2020). Green Synthesis and Characterization of Copper Oxide Nanoparticles Using Psidium guajava Leaf Extract. *IOP Conference Series: Materials Science and Engineering*, *961*(1). https://doi.org/10.1088/1757-899X/961/1/012011

Vijaylaxmee Mishra, R.S., Nakuleshawar Dut Jasuja, D. K. G. (2014). a Review on Green Synthesis of Nanoparticles and Evaluation of Antimicrobial. *Journal of Green and Herbal Chemistry*, *7*(1), 52–58.

Wagener, P., Jakobi, J., Rehbock, C., Chakravadhanula, V. S. K., Thede, C., Wiedwald, U.,

Bartsch, M., Kienle, L., & Barcikowski, S. (2016). Solvent-surface interactions control the phase structure in laser-generated iron-gold core-shell nanoparticles. *Scientific Reports*, *6*(November 2015), 1–12. https://doi.org/10.1038/srep23352

Whitesides, G. M. (2005). Nanoscience, nanotechnology, and chemistry. *Small*, *1*(2), 172–179. https://doi.org/10.1002/smll.200400130

Xia, Y., Gilroy, K. D., Peng, H., & Xia, X. (2017). Keimvermitteltes Wachstum kolloidaler Metallnanokristalle. *Angewandte Chemie*, *129*(1), 60–98. https://doi.org/10.1002/ange.201604731

Yadi, M., Mostafavi, E., Saleh, B., Davaran, S., Aliyeva, I., Khalilov, R., Nikzamir, M., Nikzamir, N., Akbarzadeh, A., Panahi, Y., & Milani, M. (2018). Current developments in green synthesis of metallic nanoparticles using plant extracts: a review. *Artificial Cells, Nanomedicine and Biotechnology*, *46*(sup3), S336–S343. https://doi.org/10.1080/21691401.2018.1492931

Zhang, D., Ma, X., Gu, Y., Huang, H., & Zhang, G. (2020). *Green Synthesis of Metallic Nanoparticles and Their Potential Applications to Treat Cancer*. *8*(October), 1–18. https://doi.org/10.3389/fchem.2020.00799